Supplementary Information for

Nanoparticle Superlattices through Template-Encoded DNA Dendrimers

Ho Fung Cheng, [‡,†] Max E. Distler, [‡,†] Byeongdu Lee,[#] Wenjie Zhou,[†] Steven Weigand,[§] and Chad A. Mirkin*[,†]

† Department of Chemistry and International Institute for Nanotechnology, Northwestern University, Evanston, Illinois 60208, United States.

X-ray Science Division, Advanced Photon Source, Argonne National Laboratory, Lemont, Illinois 60439, United States.

§ DuPont−Northwestern−Dow Collaborative Access Team (DND-CAT) Synchrotron Research Center, Northwestern University, Argonne, Illinois 60208, United States.

[‡]These authors contributed equally to this work.
*Corresponding author. Email: chadnano@northwestern.edu

Table of Contents

Materials and Methods

Synthesis of oligonucleotides and DNA-containing structures

Reagents and solid-phase supports were purchased from Glen Research. Linear oligonucleotides were synthesized using a MerMade 12 synthesizer (Bio Automation) on controlled pore glass (CPG) beads (Universal UnyLinker Support (1000 Å)), using conditions recommended by the manufacturer. DNA dendrons were synthesized using a modified coupling protocol reported previously.[1] Specifically, they were synthesized using an ABI synthesizer on a dT CPG (2000 Å) with 2× phosphoramidite concentration. DNA-containing templates were synthesized *via* solid-phase click coupling,[2] following reported procedures.[3] All constructs were cleaved from the solid-phase support and deprotected by treating the support with AMA (ammonium hydroxide/40 % aqueous methylamine 1:1 v/v) at 55 °C for 30 min. Linear oligonucleotides were purified using reverse-phase high-performance liquid chromatography (RP-HPLC; Agilent), while other DNA-containing constructs were purified using denaturing polyacrylamide gel electrophoresis (PAGE). The samples were characterized using matrix-assisted laser desorption/ionization-time of flight (MALDI-TOF; AutoFlex-III, Bruker) mass spectrometry (matrix: dihydroxyacetone phosphate). A complete list of synthesized oligonucleotides can be found in Tables S1-3. The concentrations of DNA dendrons and DNA-containing templates were determined by measuring the solution absorbance at $\lambda = 260$ nm (Cary 5000 UV-vis spectrophotometer, Varian) and using the extinction coefficients calculated by the OligoAnalyzer tool (Integrated DNA Technologies).

Polyacrylamide gel electrophoresis (PAGE) purification and characterization

Gel stock solution was prepared at 1× Tris/Borate/EDTA (TBE) (EDTA: ethylenediaminetetraacetic acid) and diluted to the desired acrylamide concentration (4.5–12 %). For a denaturing gel, the solution was made to 6 M urea. Ammonium persulfate (2 mg) and tetramethylethylenediamine (15 µL) were added to the stock solution (15 mL) before it was cast between two pre-assembled glass plates. The samples were loaded in amounts that corresponded to ~ 0.012 optical density (OD) for analytical gels. The sample solutions were made up to 6 M urea for denaturing PAGE; glycerol was added instead of urea as a density modifier for native PAGE. Submerged in 1× TBE buffer, the gel was run at 8 V/cm. For purification, bands were visualized under a UV lamp, excised, crushed, and extracted into water over two days at room temperature. The extractant was then desalted and lyophilized. For analytical gels, bands were visualized using GelRed stain and imaged on a ChemiDoc imager. Images that show the entire gels are included in Figure S16.

DNA functionalization of AuNPs

10-nm gold nanoparticles (AuNPs) were purchased from Ted Pella and used as received. The 5' thiolated "PAE anchor" (Table S1) was activated as follows: 100 mM dithiothreitol (DTT) in 170 mM Na_3PO_4 (pH~7.0–8.0, 0.8 mL) was added to 40 OD of PAE anchor. After 1 h, excess DTT was removed using a size exclusion column (NAP-10), and the eluent was added to AuNPs (40 mL). After a brief vortexing step, the AuNP solution was incubated at room temperature. After 2 h, 1% SDS (0.4 mL) was added to prevent subsequent nanoparticle aggregation. After 20 min, 1 M phosphate-buffered saline (PBS, pH = 8, 0.4 mL) was added to the AuNP solution, which was vortexed and sonicated briefly. After 30 min, using a stock solution of 5 M NaCl, the AuNP solution was brought up to 0.5 M NaCl over seven additions. The AuNP solution was left standing for 25 min between each salt addition to allow a dense functionalization of the nanoparticle surface with DNA strands. Then, the AuNP solution was shaken at 100 rpm for two days in

the dark. The AuNPs were concentrated and purified using centrifugal filters (100 kDa) to remove excess, free DNA strands. The AuNPs were washed thoroughly with 0.02% SDS (2× 10 mL) and water (3× 10 mL), and the concentration of the AuNPs was determined by measuring the absorbance at 520 nm using UV-vis spectroscopy. The DNA-functionalized AuNPs were stored in the dark in a refrigerator at 4 °C prior to use. The 5-nm AuNPs were functionalized in an identical manner.

Synthesis of nanoparticle superlattices

A solution of a linker strand (200 equivalents) bearing a 5' AAGGAA 3' sticky end was added to a solution of 10-nm AuNPs functionalized with a complementary, thiolated anchor strand. This solution was added to a solution of supramolecular DNA dendrimers, in the specified dendron/AuNP ratios (typically 16:1 or 24:1), and they were made up to 100 μL at 0.5 M NaCl, 10 mM phosphate, and 0.015% SDS (Table S5), unless otherwise specified (Table S6). Aggregates formed within 30 min at room temperature, and the resulting suspensions were heated to 60 °C, above the crystals' melting temperatures, and cooled to 22 °C at a rate of 0.1 °C per 10 min, using a PCR thermal cycler (Applied Biosystems).

Dynamic light scattering (DLS) measurements

Samples were dissolved at 2.5 to 7.5 mM in a pH 7.4 buffer (70 μL) with 0.5 M NaCl, 10 mM phosphate, and the specified SDS concentrations. Triplicate measurements were taken at 25 °C on a Zetasizer Nano ZS (Malvern Panalytical). Data was fitted on a monomodal distribution, using a refractive index of 1.48 and solution viscosity of 0.9345, on Zetasizer Nano Software (Malvern Panalytical).

Generating 3D models and movies of DNA dendrimers and micelle-dendrimers

Organic cores and surfactants were modelled atomistically and drawn to scale. DNA was modelled as helical backbone, while flexible spacers were rendered as ethylene glycol repeating units. All 3D models and movies were created using Cinema 4D™ (Maxon).

UV-vis melt experiment for determining the thermostabilities of superlattices

To obtain the melting temperature, a suspension of a sample (120 μL) was diluted to 0.7 mL using a pH 7.4 buffer with 0.5 M NaCl, 10 mM phosphate, 0.015% SDS and transferred to a UV-vis cuvette with a magnetic stir bar and a cap. The sample was heated at a ramp rate of 0.1 °C/min while the absorbance at 520 nm was measured. Alpha (α) curves, first derivative plots, and melting temperatures (T_m) were generated from the data using the Varian Thermal Application software.

Fluorescence plate reader diffusivity measurements

For an accurate assessment of diffusivity, superlattices were synthesized using Cy3-labeled and Cy3-free dendrons (6Dn' and 6Dn_v2, Table S3) with an identical number of sticky ends. The DNA sequences on their stems are also uniquely complementary to their respective templates (Table S4), such that the results of the diffusion experiments would not be confounded by linker-anchor exchange. The synthesized

nanoparticle superlattice suspensions were washed three times with assembly buffer to remove excess AuNPs, dendrons, or dendrimers. The initial fluorescence intensities of the assembly solution were measured using a fluorescence plate reader (Biotek Cytation 5 Imaging Reader) by transferring 50 µL of supernatant to a 96-well plate. Immediately following measurement, the 50 µL samples were returned to their respective containers. DNA dendrons and dendrimers that were not fluorescently labeled were added to the nanoparticle superlattice suspensions, thereby creating a DNA dendron/dendrimer concentration gradient. Several fluorescence intensity measurements were taken at specific timepoints to track the diffusion of fluorescently labeled DNA dendrons/dendrimers from the nanoparticle superlattice to the surrounding solution. All diffusivity experiments were conducted at room temperature.

Small-angle x-ray scattering (SAXS) characterization

SAXS data were collected in beamlines 5ID-D (DuPont-Northwestern-Dow Collaborative Access Team) and 12-ID-B of the Advanced Photon Source at Argonne National Laboratory. Using synchrotron x-rays with radiation energies of 10–13 keV, the samples were exposed for 0.1 to 1 s, and the scattered beam was collected on a CCD detector. The data were azimuthally averaged to yield one-dimensional spectra, which were plotted as scattering intensities $I(q)$, on a logarithmic scale, against the scattering vector q.

SAXS indexing and simulation

One-dimensional SAXS spectra were indexed to identify crystallographic symmetries and lattice parameters.[4] To simulate the SAXS spectra, unit cell models were constructed with spherical 10-nm AuNPs arranged in the specified phase symmetry and lattice parameters, such that all SAXS peaks are matched (Figure S17-22). The particle size (diameter = 9.5 ± 0.5 nm), polydispersity factor (5–10%), average crystalline domain size, Debye-Waller factor (DWF), and micro-strain parameter were empirically adjusted to match the widths and intensities of the peaks across the spectrum. The MATLAB script package is available at https://sites.google.com/site/byeongdu/software.

Silica encapsulation, resin embedding, and ultramicrotomy

Nanoparticle superlattices were encapsulated in silica following a reported procedure.[5] The precipitates were transferred to a 0.5 M NaCl, 10 mM phosphate buffer (0.3 mL). N-trimethoxysilylpropyl-N,N,N-trimethylammonium chloride (2 µL) was added to this suspension, which was then shaken at 850 rpm at 18 °C for 1 h. Then, triethoxysilane (4 µL) was added, and the suspension was shaken at 850 rpm at 18 °C overnight. Excess silica was removed, and the superlattices were suspended and washed with water (3× 200 µL), and then ethanol (2× 200 µL). The silica-encapsulated samples were drop-cast onto a TEM grid for morphological characterization. To obtain cross-sections of the superlattices, the silica-encapsulated samples were then embedded in resin and ultramicrotomed into thin slices following a reported procedure.7 In short, 4% gelatin solution (0.15 mL) was added to dried, silica-encapsulated samples. The gelatin solution was frozen under liquid nitrogen, and the gelatin block was submerged in 1.5 mL of the following, for two cycles, with 10-min incubations at 100 rpm: 30% EtOH, 50% EtOH, 70% EtOH, 80% EtOH, 90% EtOH, 100% EtOH, acetone. EMBed-812 resin (Electron Microscopy Sciences) was prepared by combining dodecenyl succinic anhydride (9 g), EMBed-812 (22.6 g) and NADIC methyl anhydride (14.7 g). After removing the acetone, 1:1 acetone/resin (1.5 mL) was added, and the sample was incubated overnight at 100 rpm. The solvent was then exchanged into 1:3 acetone/resin (1.5 mL) and incubated at 100 rpm for 1 h, followed by 2 h of open-vial incubation to evaporate the acetone. The gelatin block was

exchanged into fresh resin for two days, and then exchanged into a resin mixture with crosslinker (0.7 g DMP-30) and heated overnight at 65 °C for curing. The resin block was sectioned into 80-nm slices (Leica EM UC7), and these slices were placed on copper-grided TEM grids with ~20-nm carbon films.

Scanning transmission electron microscopy (STEM) characterization

Silica-encapsulated or ultramicrotome-sectioned samples were deposited on carbon film-coated copper grids (Ted Pella) and loaded onto a double-tilt sample holder for STEM imaging. Annular dark field (ADF), annular bright-field (ABF), and secondary electron (SE) imaging were performed on a Hitachi HD-2300A with a field emission gun operated at 200 kV. Models of the lattice and their 2D projections were created using the Diamond software (Crystal Impact), after inputting the space groups and lattice parameters. All electron micrographs reported in the manuscript were unmodified, other than being cropped for clarity. Uncropped images can be found in Figure S23-28.

Voronoi polyhedra analysis

Models of unit cells were generated using space groups and lattice parameters determined from SAXS experiments. Voronoi polyhedra were generated using the locations of AuNPs (Figure 4a) to elucidate the positions of DNA micelle-dendrimers. Voronoi polyhedra were also generated using the locations of both AuNPs and DNA micelle-dendrimers (Figure S12). The figures were generated, and the subsequent structural analyses were performed, using Diamond (Crystal Impact).

Acronyms for phosphoramidites:

Sp18: 18-*O*-Dimethoxytritylhexaethyleneglycol,1-[(2-cyanoethyl)-(*N*,*N*-diisopropyl)]-phosphoramidite (Spacer phosphoramidite 18)

Thiol: 1-*O*-Dimethoxytrityl-hexyl-disulfide,1'-[(2-cyanoethyl)-(*N*,*N*-diisopropyl)]-phosphoramidite (Thiol-modifier C6 S-S)

DBCO: 10-(6-oxo-6-(dibenzo[b,f]azacyclooct-4-yn-1-yl)-capramido-*N*-ethyl)-*O*-triethyleneglycol-1-[(2-cyanoethyl)-(*N*,*N*-diisopropyl)]-phosphoramidite (5'-DBCO-TEG phosphoramidite)

Hexynyl: 5-Hexyn-1-yl-(2-cyanoethyl)-(N,N-diisopropyl)-phosphoramidite (5'-Hexynyl phosphoramidite)

D: 1,3-bis-[5-(4,4'-dimethoxytrityloxy)pentylamido]propyl-2-[(2-cyanoethyl)-(*N*,*N*-diisopropyl)]-phosphoramidite (Symmetric doubler phosphoramidite)

Tr: Tris-2,2,2-[3-(4,4'-dimethoxytrityloxy)propyloxymethyl]methyleneoxypropyl-[(2-cyanoethyl)-(*N*,*N*-diisopropyl)]-phosphoramidite (Long trebler phosphoramidite)

Cy3: 1-[3-(4-monomethoxytrityloxy)propyl]-1'-[3-[(2-cyanoethyl)-(*N*,*N*-diisopropyl) phosphoramidityl]propyl]-3,3,3',3'-tetramethylindocarbocyanine chloride (Cyanine 3 phosphoramidite)

Experimental Details

DNA Design and Characterization

Table S1. Linear oligonucleotides synthesized for this study.

	DNA Sequence (5' to 3')	Calc'd MW	Exp't MW
PAE anchor	Thiol-$(Sp18)_2$-AACGACTCATACTCACCT	6,403	6,425
PAE linker	AAGGAA-Sp18-AGGTGAGTATGAGTCGTT	7,834	7,869
Temp_v1 (DBCO)	DBCO-$(Sp18)_2$-TGGAGTGAATGGTAATAGTGAGTGGT	9,444	9,445
Temp_v1 (hexynyl)	Hexynyl-$(Sp18)_2$-TGGAGTGAATGGTAATAGTGAGTGGT	9,034	9,036
Temp_v2 (DBCO)	DBCO-$(Sp18)_2$-CATCCATCCTTATCAACT	6,613	6,618
Deactivating strand	AACATCTAATCTACATCTACCACTCACTATTACCATTCACTCCA	13,218	13,234
Activating strand	TGGAGTGAATGGTAATAGTGAGTGGTAGATGTAGATTAGATGTT	13,840	13,879
Rigidifying strand	TAGGTTGATAAG	3,725	3,776

Table S2. DNA templates synthesized for this study.

	Template arm sequence	Coupling yield* (%)	Calc'd MW (kDa)	Exp't MW (kDa)
T2	Temp_v1 (DBCO)	41	19.1	19.0
T3	Temp_v1 (DBCO)	64	28.6	28.5
T4	Temp_v1 (DBCO)	27	38.3	38.2
T6	Temp_v1 (DBCO)	23	57.5	59.5
T8	Temp_v1 (DBCO)	9	77.7	78.5
T8'	Temp_v1 (hexynyl)	7	74.4	72.6
T2_v2	Temp_v2 (DBCO)	50	13.4	13.7
T4_v2	Temp_v2 (DBCO)	54	26.9	27.1
T6_v2	Temp_v2 (DBCO)	23	40.5	41.0

*Coupling yield is calculated by dividing the amount of DNA templates isolated by the theoretical maximum that could be synthesized, taking into account that ~30% of the chains are not terminated. A typical coupling reaction yields ~30-40 nmol of isolated product, sufficient for preparing more than 5,000 assemblies under the conditions described in this work.

Table S3. DNA dendrons synthesized for this study.

	DNA Sequence (5' to 3')	Isolated yield** (%)	Calc'd MW (kDa)	Exp't MW (kDa)
3Dn*	TTCCTT-Sp18-Tr-Sp18-Cy3-Sp18-ACCACTCACTATTACCATTCCTT	7	14.9	14.9
4Dn*	TTCCTT-Sp18-D-Sp18-D-Sp18-Cy3-Sp18-ACCACTCACTATTACCATTCCTT	9	18.4	18.3
6Dn*	TTCCTT-Sp18-D-Sp18-Tr-Sp18-Cy3-Sp18-ACCACTCACTATTACCATTCCTT	4	23.4	23.1
6Dn'	TTCCTT-Sp18-D-Sp18-Tr-Sp18-Cy3-Sp18-ACCACTCACTATTACCAT	3	21.9	21.6
6Dn-L1	TTCCTT-Sp18-D-Sp18-Tr-Sp18-Cy3-Sp18-TCAACCTAACCACTCACTATTACCAT	4	24.3	24.0
6Dn-L2	TTCCTT-Sp18-D-Sp18-Tr-Sp18-Cy3-Sp18-CTTATCAACCTAACCACTCACTATTACCAT	5	25.5	25.2
6Dn-L3	TTCCTT-Sp18-D-Sp18-Tr-Sp18-Cy3-Sp18-CTTATCAACCTAACCACTCACTATTACCATTCACT	8	27.0	26.7
6Dn_v2	TTCCTT-Sp18-D-Sp18-Tr-Sp18-AGTTGATAAGGATGGAT	1***	21.0	22.0

*A 5' TTCCTT 3' sequence was appended at the 3' end of 3Dn, 4Dn, and 6Dn to augment dendron-AuNP PAE interactions. This modification improved the crystallinities and thermostabilities of the dendron-PAE assemblies, presumably by mitigating the repulsive contributions of the long stem regions.

**Assuming a coupling efficiency of 97%, a linear, 40-base DNA synthesis would be at ~20% isolated yield post-purification. The dendritic architecture and incorporation of specialty phosphoramidites decrease the synthetic yield. A standard 10-μmol synthesis would yield ~400 nmol of DNA dendrons, sufficient for preparing more than 9,000 assemblies under the conditions described in this work.

***Low isolated yield due to accidental operational loss.

Table S4. Calculated melting temperatures (T_m) of anchor-linker pairs.

	DNA Sequence (5' to 3')*	T_m / °C*
PAE anchor	Thiol-$(Sp18)_2$-**AACGACTCATACTCACCT**	65
PAE linker	AAGGAA-Sp18-**AGGTGAGTATGAGTCGTT**	
Temp_v1 (DBCO)	DBCO-$(Sp18)_2$-**TGGAGTGAATGGTAATAGTGAGTGGT**	64
6Dn	TTCCTT-Sp18-D-Sp18-Tr-Sp18-Cy3-Sp18-**ACCACTCACTATTACCATTCCTT**	
Temp_v1 (DBCO)	DBCO-$(Sp18)_2$-**TGGAGTGAATGGTAATAGTGAGTGGT**	62
6Dn’	TTCCTT-Sp18-D-Sp18-Tr-Sp18-Cy3-Sp18-**ACCACTCACTATTACCAT**	
Temp_v1 (DBCO)	DBCO-$(Sp18)_2$-**TGGAGTGAATGGTAATAGTGAGTGGT**	62
6Dn-L1	TTCCTT-Sp18-D-Sp18-Tr-Sp18-Cy3-Sp18-**TCAACCTAACCACTCACTATTACCAT**	
Temp_v1 (DBCO)	DBCO-$(Sp18)_2$-**TGGAGTGAATGGTAATAGTGAGTGGT**	62
6Dn-L2	TTCCTT-Sp18-D-Sp18-Tr-Sp18-Cy3-Sp18-**CTTATCAACCTAACCACTCACTATTACCAT**	
Temp_v1 (DBCO)	DBCO-$(Sp18)_2$-**TGGAGTGAATGGTAATAGTGAGTGGT**	69
6Dn-L3	TTCCTT-Sp18-D-Sp18-Tr-Sp18-Cy3-Sp18-**CTTATCAACCTAACCACTCACTATTACCATTCACT**	
Temp_v2 (DBCO)	DBCO-$(Sp18)_2$-**CATCCATCCTTATCAACT**	60
6Dn_v2	TTCCTT-Sp18-D-Sp18-Tr-Sp18-**AGTTGATAAGGATGGAT**	
Temp_v1 (DBCO)	DBCO-$(Sp18)_2$-**TGGAGTGAATGGTAATAGTGAGTGGT**	72
Deactivating strand	**AACATCTAATCTACATCTACCACTCACTATTACCATTCACTCCA**	
Activating strand	**TGGAGTGAATGGTAATAGTGAGTGGTAGATGTAGATTAGATGTT**	80
Deactivating strand	**AACATCTAATCTACATCTACCACTCACTATTACCATTCACTCCA**	
6Dn-L2	TTCCTT-Sp18-D-Sp18-Tr-Sp18-Cy3-Sp18-**CTTATCAACCTAACCACTCACTATTACCAT**	40
Rigidifying strand	**TAGGTTGATAAG**	

*All melting temperatures are calculated on NUPACK (http://www.nupack.org/partition/new, accessed on April 16, 2021),[6] with [oligonucleotide] = 0.3 μM, [Na^+] = 0.5 M. The inputted sequences are bolded, and the base-pairs that were hybridized at room temperature are underlined. All sequences were checked to ensure that no secondary structures were expected to form at room temperature.

Phase Space Exploration

Table S5. Phase space screening of dendron/dendrimer-templated superlattices.

Dendron	Template	Dendron/ AuNP ratio	Symmetry	Space group*	Lattice constant (nm)*	AuNP Wyckoff positions*
3Dn	N/A	16	FCC	*Fm*-3*m*	a = 42.8	4a
3Dn	T2	16	SH	*P*6/*mmm*	a = 32.3, c = 31.9	1a
3Dn	T3	16	SH	*P*6/*mmm*	a = 31.5, c = 30.9	1a
3Dn	T4	16	SH	*P*6/*mmm*	a = 31.6, c = 31.2	1a
3Dn	T6	16	SC	*Pm*-3*m*	a = 30.0	1a
3Dn	T8	16	SC, SH	*Pm*-3*m*	a = 29.3	1a
4Dn	N/A	16	FCC	*Pm*-3*m*	a = 46.1	4a
4Dn	T2	16	SH	*P*6/*mmm*	a = 32.4, c = 32.0	1a
4Dn	T3	16	SH	*P*6/*mmm*	a = 32.4, c = 32.0	1a
4Dn	T4	16	SH	*P*6/*mmm*	a = 33.3, c = 32.8	1a
4Dn	T6	16	SC, SH	*P*6/*mmm*	a = 33.3, c = 32.8	1a
4Dn	T8	16	SC, SH	*Pm*-3*m*	a = 31.3	1a
6Dn	N/A	16	FCC	*Fm*-3*m*	a = 45.5	4a
6Dn	T2	16	SH	*P*6/*mmm*	a = 32.6, c = 32.6	1a
6Dn	T3	16	SH	*P*6/*mmm*	a = 32.0, c = 32.4	1a
6Dn	T4	16	SH**	*P*6/*mmm*	a = 32.4, c = 32.1	1a
6Dn	T6	16	SC	*Pm*-3*m*	a = 30.6	1a
6Dn	T8	16	SC	*Pm*-3*m*	a = 31.3	1a
6Dn-L1	N/A	24	FCC	*Fm*-3*m*	a = 45.2	4a
6Dn-L1	T2	24	Ti_5Ga_4	*P*63/*mcm*	a = 72.3, c = 61.1	4d, 6g
6Dn-L1	T3	24	Ti_5Ga_4	*P*63/*mcm*	a = 72.3, c = 61.1	4d, 6g
6Dn-L1	T4	24	SC	*Pm*-3*m*	a = 30.2	1a
6Dn-L1	T6	24	SC	*Pm*-3*m*	a = 30.9	1a
6Dn-L1	T8	24	SC	*Pm*-3*m*	a = 30.7	1a
6Dn-L2	N/A	24	FCC	*Fm*-3*m*	a = 47.0	4a
6Dn-L2	T2	24	Ti_5Ga_4	*P*63/*mcm*	a = 73.0, c = 61.4	4d, 6g
6Dn-L2	T3	24	Ti_5Ga_4	*P*63/*mcm*	a = 72.7, c = 60.5	4d, 6g
6Dn-L2	T4	24	SC	*Pm*-3*m*	a = 31.0	1a
6Dn-L2	T6	24	GT, SC	*Pm*-3*m*	a = 31.6	1a
6Dn-L2	T8	24	GT, SC	*Pm*-3*m*	a = 31.2	1a
6Dn-L3	N/A	16	FCC	*Fm*-3*m*	a = 46.1	4a
6Dn-L3	T2	24	Ti_5Ga_4	*P*63/*mcm*	a = 73.2, c = 61.5	4d, 6g
6Dn-L3	T3	24	Ti_5Ga_4, SC	*P*63/*mcm*	a = 75.3, c = 62.7	4d, 6g
6Dn-L3	T4	24	Ti_5Ga_4, SC	*Pm*-3*m*	a = 31.1	1a
6Dn-L3	T6	24	GT, SC	*P*6/*mmm*	a = 36.0, c = 36.5	2d

6Dn-L3	T8	24	GT, SC	*P6/mmm*	a = 38.1, c = 36.7	2d

Assembly buffer: 0.5 M NaCl, 10 mM phosphate, 0.015 % SDS, pH 7.4.
200 equiv. of PAE linker strands were added per AuNP PAE (25 nM).
*The major phase's space group, lattice parameters, and AuNP Wyckoff positions are reported.
**This sample contains some partially disordered *R*-3*m* phase.

Table S6. Effect of changing SDS concentration.

Dendron	Template	Dendron/ AuNP ratio	SDS (%)	Symmetry *	Space group*	Lattice constant (nm)*
4Dn	T2	16	0	disordered	N/A	N/A
4Dn	T2	16	0.005	disordered	N/A	N/A
4Dn	T2	16	0.01	**SC, SH**	*P6/mmm*	a = 33.1, c = 32.8
4Dn	T2	16	0.02	SH	*P6/mmm*	a = 32.3, c = 32.0
4Dn	T2	16	0.04	SH	*P6/mmm*	a = 32.3, c = 32.0
6Dn	T6	16	0	SH (br)	*P6/mmm*	a = 31.7, c = 31.7
6Dn	T6	16	0.005	SH (br)	*P6/mmm*	a = 31.7, c = 31.7
6Dn	T6	16	0.01	**SC**	*Pm-3m*	a = 30.8
6Dn	T6	16	0.02	SC, SH	*Pm-3m*	a = 30.8
6Dn	T6	16	0.04	SC, SH	*Pm-3m*	a = 30.7
6Dn	T3	24	0	SH (br)	*P6/mmm*	a = 32.2, c = 31.7
6Dn	T3	24	0.005	SH (mixed)	*P6/mmm*	a = 32.0, c = 31.9
6Dn	T3	24	0.01	**SC**	*Pm-3m*	a = 31.0
6Dn	T3	24	0.02	SH	*P6/mmm*	a = 32.3, c = 32.1
6Dn**	T3	24	0.04	SH	*P6/mmm*	a = 32.3, c = 32.1
6Dn-L2	T3	24	0	SH	*P6/mmm*	a = 32.2, c = 32.0
6Dn-L2	T3	24	0.005	SH	*P6/mmm*	a = 32.3, c = 32.1
6Dn-L2	T3	24	0.01	**Ti_5Ga_4**	*P63/mcm*	a = 73.5, c = 60.6
6Dn-L2	T3	24	0.02	Ti_5Ga_4 (br)	*P63/mcm*	a = 73.4, c = 60.9
6Dn-L2	T3	24	0.04	SC	*Pm-3m*	a = 33.7

The phases formed around the CMC of SDS (0.01%) are bolded. All assemblies are prepared in 0.5 M NaCl, 10 mM phosphate, pH 7.4.
*The major phase's space group and lattice parameters are reported.
**Above the critical micelle concentration (CMC), all additional SDS surfactant molecules would be incorporated into micelles. Therefore, more than three quarters of the SDS molecules are incorporated into micelles at a SDS concentration of 0.04%. Since SDS micelles have an average aggregation number of ~148 at 0.5 M NaCl,[7] the concentration of SDS micelles would be larger than 0.7 μM. For this assembly condition, the concentration of DNA dendrimer (made up one T3 and three 6Dn) is 0.2 μM, which is significantly lower than the estimated concentration of SDS micelles. Thus, these conditions would favor less dendrimer-dendrimer association as the dendrimers can be divided among many micelles.

Table S7. Comparing the observed nanoparticle superlattice Ti_5Ga_4-type phase (upper) with the intermetallic structure Ti_5Ga_4 (bottom).[8-9] Coord.: coordination. CN: coordination number. The coordination distances to the bolded atoms are included for the intermetallic structure Ti_5Ga_4.

Site	Wyckoff position	Coordinates	Coord.	Coord. distances (Å)	Coord. partners	Polyhedra CN	Polyhedra vol (10^6 Å^3)
AuNP1	4d	1/3, 2/3, 0	Den_6	271	Six 6g	14	16.5
AuNP2	6g	1/4, 0, 1/4	Den_7	237	Two 2b	17	15.8
				259	Three 6g		
				317	Two 6g		
Den1	2b	0, 0, 0	$AuNP_6$	237	Six 6g	14	12.9
Den2	6g	3/5, 0, 1/4	$AuNP_9$	259	Four 4d	13	15.9
				271	Three 6g		
				317	Two 6g		

Site	Wyckoff position	Coordinates	Coord.	Coord. distances (Å)	Coord. partners	Polyhedra CN	Polyhedra vol (Å^3)
Ti1	4d	1/3, 2/3, 0	Ti_8**Ga$_6$**	2.81	Six 6g	14	16.4
Ti2	6g	0.29, 0, 1/4	Ti_8**Ga$_7$**	2.66	Two 2b	15	16.3
				2.59	One 6g		
				2.70	Two 6g		
				2.82	Two 6g		
Ga1	2b	0, 0, 0	**Ti$_6$**Ga_6	2.66	Six 6g	14	15.6
Ga2	6g	0.62, 0, 1/4	**Ti$_9$**Ga_4	2.81	Four 4d	13	16.1
				2.69	One 6g		
				2.70	Two 6g		
				2.82	Two 6g		

Table S8. Effect of rigidifying the dendron stem.

Dendron	Template	Rigidifying strand	Symmetry	Space group*	Lattice constant (nm)*
6Dn-L2	T2	-	Ti_5Ga_4	*P*63/*mcm*	a = 73.0, c = 61.4
6Dn-L2	T2	+	Ti_5Ga_4	*P*63/*mcm*	a = 74.7, c = 60.6
6Dn-L2	T3	-	Ti_5Ga_4	*P*63/*mcm*	a = 72.7, c = 60.5
6Dn-L2	T3	+	Ti_5Ga_4	*P*63/*mcm*	a = 75.3, c = 60.1
6Dn-L2	T6	-	GT, SC	*Pm*-3*m*	a = 31.6
6Dn-L2	T6	+	GT, SC	*P*6/*mmm***	a = 38.0, c = 36.7
6Dn-L2	T8	-	GT, SC	*Pm*-3*m*	a = 31.2
6Dn-L2	T8	+	GT, SC	*P*6/*mmm***	a = 38.1, c = 36.7
6Dn-L3	T2	-	Ti_5Ga_4	*P*63/*mcm*	a = 73.2, c = 61.5
6Dn-L3	T2	+	Ti_5Ga_4	*P*63/*mcm*	a = 76.0, c = 51.0
6Dn-L3	T6	-	GT, SC	*P*6/*mmm*	a = 36.0, c = 36.5

6Dn-L3	T6	+	GT, SC	*P6/mmm***	a = 36.4, c = 37.4
6Dn-L3	T8	-	GT, SC	*P6/mmm*	a = 38.1, c = 36.7
6Dn-L3	T8	+	GT, SC	*P6/mmm***	a = 38.1, c = 36.9

Assembly buffer: 0.5 M NaCl, 10 mM phosphate, 0.015% SDS, pH 7.4.
*The major phase's space group and lattice parameters are reported.
**The amount of GT phase increases slightly upon the addition of the rigidification strand. The rigidification of the dendron stem likely leads to the branching regions being situated further apart from each other in micelle-dendrimers.

Table S9. Effect of changing assembly stoichiometry. Most structures, as defined by phase symmetries, are identical at dendron/AuNP = 16:1 or 24:1.

Dendron	Template	Dendron/Au NP ratio	Symmetry	Space group*	Lattice constant (nm)*
6Dn	N/A	16	FCC	*Fm-3m*	a = 45.5
6Dn	N/A	24	FCC	*Fm-3m*	a = 44.8
6Dn	T3	16	SH	*P6/mmm*	a = 32.0, c = 32.4
6Dn	T3	24	SH	*P6/mmm*	a = 32.4, c = 32.1
6Dn	T6	16	SC	*Pm-3m*	a = 30.6
6Dn	T6	24	SC	*Pm-3m*	a = 30.6
6Dn-L2	T3	16	Ti_5Ga_4 (br)**	*P63/mcm*	a = 73.5, c = 61.3
6Dn-L2	T3	24	Ti_5Ga_4	*P63/mcm*	a = 72.7, c = 60.5
6Dn-L3	T6	16	SC***	*Pm-3m*	a = 31.3
6Dn-L3	T6	24	GT, SC	*P6/mmm*	a = 36.0, c = 36.5

Assembly buffer: 0.5 M NaCl, 10 mM phosphate, 0.015% SDS, pH 7.4.
*The major phase's space group and lattice parameters are reported.
**Lower equivalents of dendrons led to broadened SAXS spectra, consistent with our hypothesis that dendrons with a long stem region enable a higher degree of dendrimer-dendrimer association, and thus when an insufficient amount of dendrimers was added, partially disordered phases form.
***In a similar vein, a lack of dendrimers disfavors the formation of GT phase.

Additional Data and Analsysis

MALDI-TOF MS Spectra

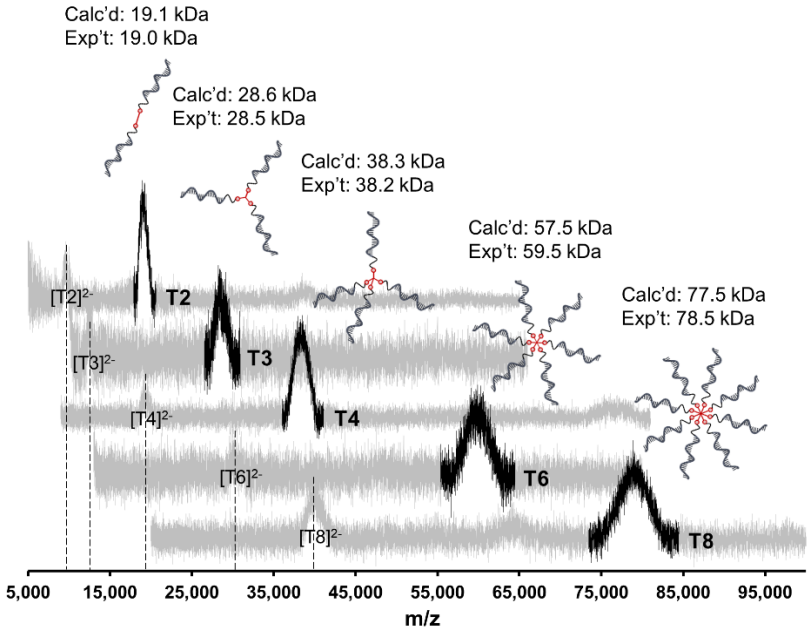

Figure S1. Stacked MALDI-TOF MS spectra of the DNA templates utilized in this work (linear and negative ion mode; matrix: dihydroxyacetone phosphate). For each spectrum, a peak at lower m/z that corresponds to a doubly charged species was assigned accordingly.

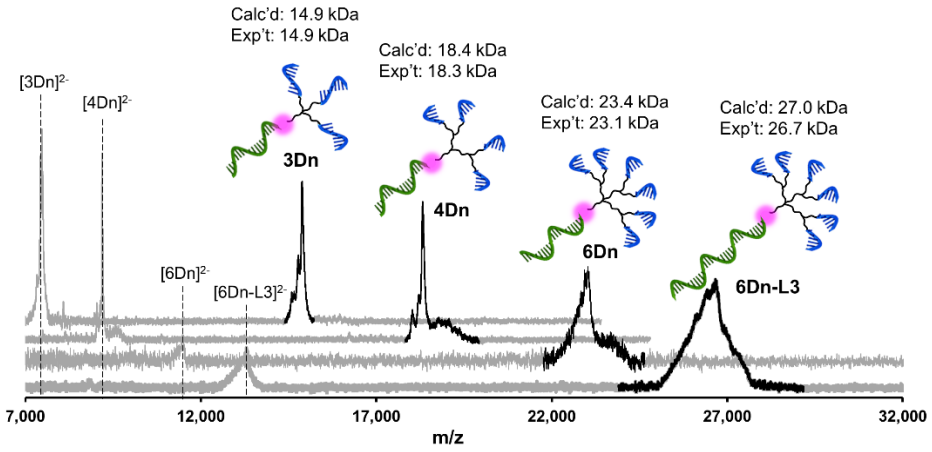

Figure S2. Stacked MALDI-TOF MS spectra of selected DNA dendrons utilized in this work (linear and negative ion mode; matrix: dihydroxyacetone phosphate). For each spectrum, a peak at lower m/z that corresponds to a doubly charged species was assigned accordingly.

Partially Disordered *R*-3*m* Phase

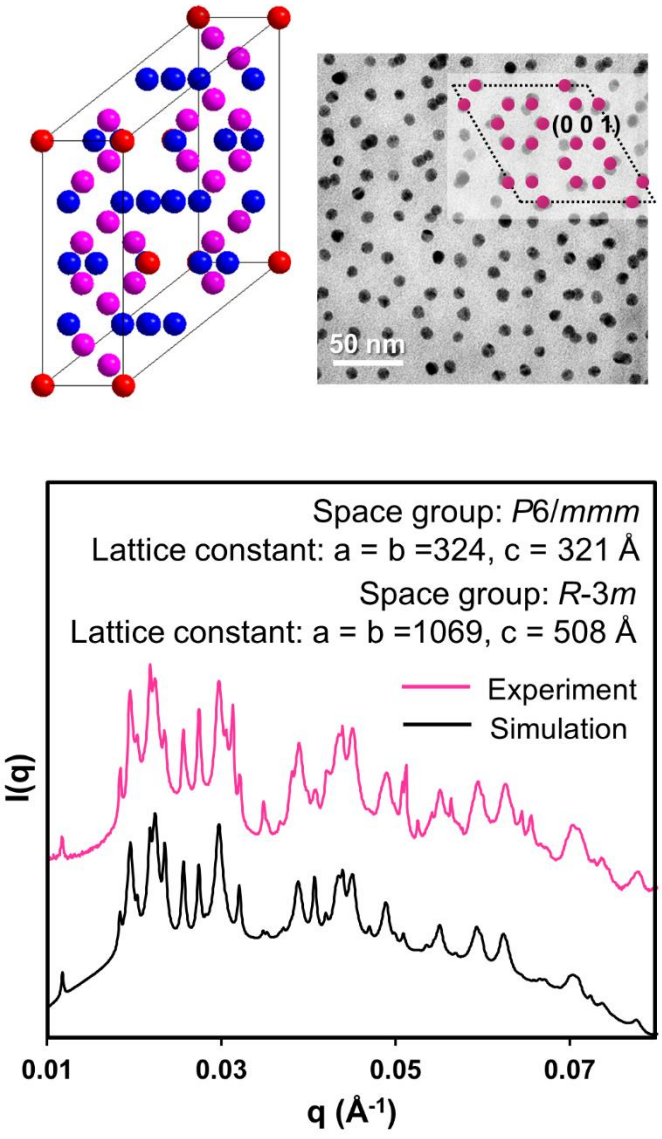

Figure S3. A mixture of SH and partially disordered *R*-3*m* phases. Top left: A structural model of the *R*-3*m* phase generated using all three Wyckoff positions. Top right: Cross-sectional ADF-STEM image shows a section where only the 18g Wyckoff position is occupied. Bottom: SAXS spectrum (pink) and simulation (black). The simulation was generated by summing contributions from a modeled SH structure and a modeled structure with *R*-3*m* phase, the latter of which was generated using partially occupied Wyckoff positions (bracketed are the relative contributions): 3a (1.25), 18g (0.5), 18 h (0.75).

Colloidal Bonding Character and Thermostability

To probe the bonding character of the colloidal crystals, we compared the diffusivity of DNA dendrons and dendrimers across the solution-superlattice interface, which is a proxy for their mobility and degree of delocalization within the superlattice. Their diffusion can be tracked by first creating a concentration gradient whereby Cy3-labeled constructs in the crystal would exchange with unlabeled constructs in the supernatant. Depending on the diffusivity of each construct, the Cy3 fluorescence intensity in the solution increases over time (Figure S4). We observed that the dendrons diffused very quickly, with a sharp increase in fluorescence intensity that plateaued after 1 h, indicating that they are mobile and delocalized within the superlattice. On the contrary, high-valent DNA dendrimers showed negligible increase in fluorescence intensity, consistent with their static and localized nature within the superlattice. These results show that DNA dendrons and dendrimers behave like EEs and PAEs,[10] respectively. We also observed that DNA dendrimers consisting of mid-range valences (i.e., N = 12) can be significantly more diffusive than a typical PAE, though not nearly to the same extent as a typical EE.[10]

These observations of DNA dendrimer bonding character were corroborated by analyzing the thermostability of the colloidal crystals *via* UV-vis melting experiments (Figure S4). We observed, as expected, that crystals composed of DNA dendrons (like EEs) have melting temperatures just above room temperature. However, when a template of increasing valency (to N = 12) is introduced to the system, the melting temperatures of the resulting assemblies increased significantly. As the template valency increases, the melting transitions become narrower, and the melting temperatures plateau at approximately 36 °C. Overall, these observations are consistent with the previously observed cooperative binding of DNA strands that are in close proximity.[11] Taken together, the diffusivity and thermostability data confirm that EE and PAE bonding characteristics represent a continuum that can be traversed by modulating the valency of the bonding moiety.

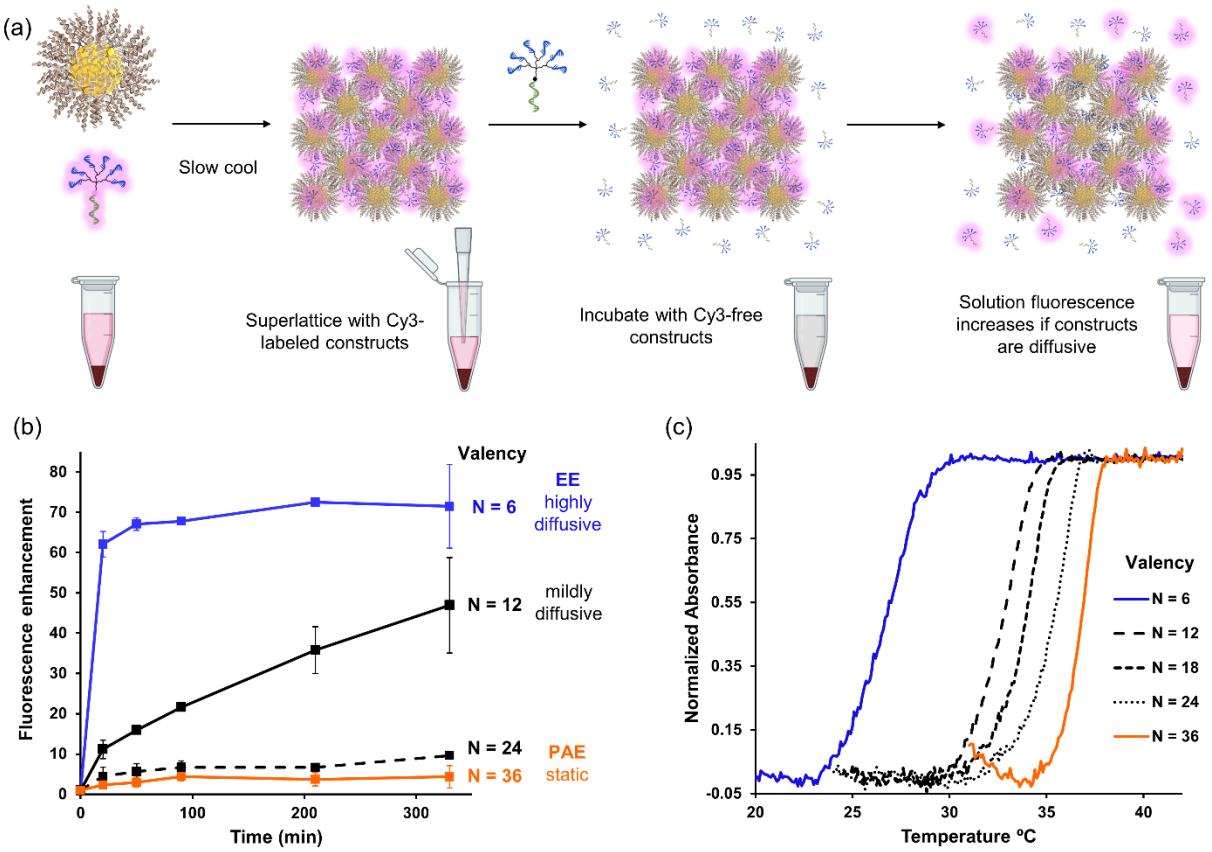

Figure S4. (a) Experimental procedures used to track the rate of diffusion of dye-labeled constructs across the solution-superlattice interface. The rate of diffusion reflects the colloidal bonding character (e.g., metallic versus ionic) of the dendrons or dendrimers in the colloidal assemblies. (b) Low-valent dendron EEs diffuse quickly while high-valent dendrimer PAEs show negligible diffusion. The amount of Cy3-labeled dendrons (6Dn') used for sample preparation, as well as the amount of non-labeled dendrons (6Dn_v2), was kept constant across different samples (24 equiv. dendrons per AuNP). The error bars denote the standard deviation in fluorescence enhancement across three independent samples. (c) The melting temperatures (T_m) increase as template valency (N) increases. For N = 6, no templates were added (i.e., only 6Dn' was used). Corresponding templates were added stoichiometrically for superlattice sample preparation for other valencies (e.g., T2 was added for N = 12).

DLS Characterization of DNA Dendrimer Association

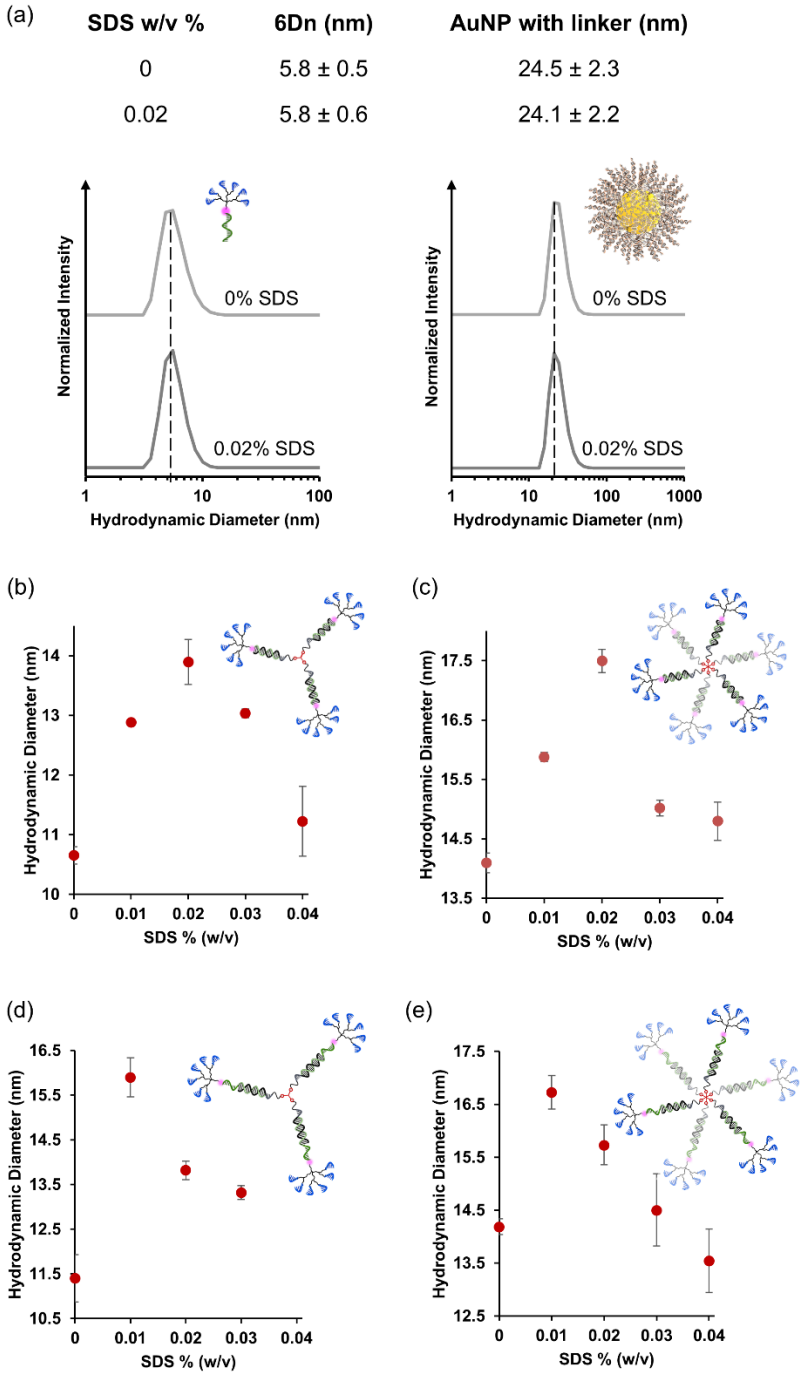

Figure S5. (a) The hydrodynamic diameters (D_h) of dendrons and AuNPs do not change with the addition of SDS in 0.5 M NaCl, 10 mM phosphate, pH 7.4 buffer. (b-e) D_h of dendrimers increase initially with SDS concentration, peak near the CMC of SDS (0.01–0.02%), and then decrease with increasing SDS concentration. Due to the dynamic nature of dendrimer-dendrimer association in solution, the increase in D_h only reflects a fraction of the increase in the size of the effective building blocks in nanoparticle

superlattices. Error bars denote the standard deviation in mean diameter from three measurements. (b) 6Dn and T3, (c) 6Dn and T6, (d) 6Dn-L2 and T3, and (e) 6Dn-L3 and T6.

Quantifying Superlattice Composition

The synthesized nanoparticle superlattice suspensions were subjected to two cycles of washing with assembly buffer to remove any AuNPs, dendrons, or dendrimers that had not been incorporated into the crystals. Water (80 µL) was added to dissolve the separated superlattice precipitates. The resulting solution was centrifuged at 15,000 rpm for 30 min to sediment the 10-nm AuNPs. The supernatant was pipetted out and added to a stock solution that was spiked with a known amount of Cy3-labeled dendrons. The stock solution absorbance at 547 nm was measured and confirmed to be within the linear detection range of the UV-vis spectrometer. After adding the supernatant, the resulting solution's absorbance at 547 nm was measured. Separately, the sedimented 10-nm AuNPs were reconstituted in water (100 µL), and the resulting solution absorbance at 520 nm was measured. The amount of Cy3-labeled dendrons and 10-nm AuNPs that had been incorporated into nanoparticle superlattices and the dendrimer/AuNP ratio could be calculated. Each quantification experiment was done in triplicate.

(a)

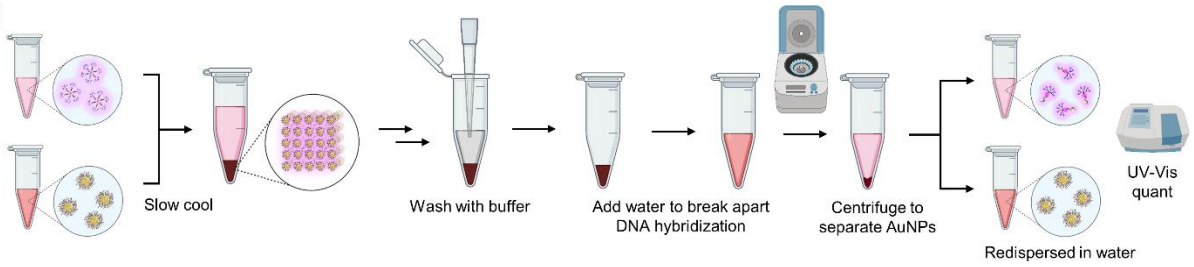

(b)

Sample	Input Dendron/AuNP	Crystal Dendron/AuNP	Structure (Stoichiometry)	No. of Dendrimers per lattice site
T3 + 6Dn	16	12.20 ± 1.09	SH (AB_2)	2.03 ± 0.18
T6 + 6Dn	16	14.13 ± 2.34	SC (AB)	2.35 ± 0.39
T8 + 6Dn	16	14.64 ± 0.99	SC (AB)	1.83 ± 0.12
T3 + 6Dn-L2	24	15.57 ± 1.14	Ti_5Ga_4-type (A_5B_4)	6.49 ± 0.48

Figure S6. (a) A typical experiment for quantifying the ratio of Cy3-labeled dendron to AuNP within a colloidal crystal sample. The crystals are washed, disassembled, and centrifuged to separate the dendrons and 10-nm AuNPs. The dendrons and AuNPs were then separately quantified using their UV-vis absorbances. (b) A table showing the composition of colloidal crystals, quantified by the ratio of dendron per gold nanoparticles. Each entry represents the average and standard deviation of three replicates. The number of dendrimers per lattice site is calculated by dividing the dendron to AuNP ratio by the template valency.

The Effect of DBCO Moieties on Crystal Structures

To confirm that hydrophobic interactions are indeed crucial to the formation of the SC phase, we synthesized a template free of hydrophobic moieties by conjugating alkynyl-appended DNA onto a polyamidoamine (PAMAM)-based octa-azide core. PAMAM is hydrophilic, and, compared to DBCOs, linear alkynes yield triazole linkages that are significantly less hydrophobic. The resulting template (denoted as T8'), free of hydrophobic moieties, was combined with 6Dn and assembled with AuNP PAE to yield SH superlattices, as predicted by the CCM. Under identical conditions, SC superlattices were formed when the DBCO-containing T8 template was used. This result confirms our hypothesis that dendrimer-dendrimer association is mediated by hydrophobic interactions.

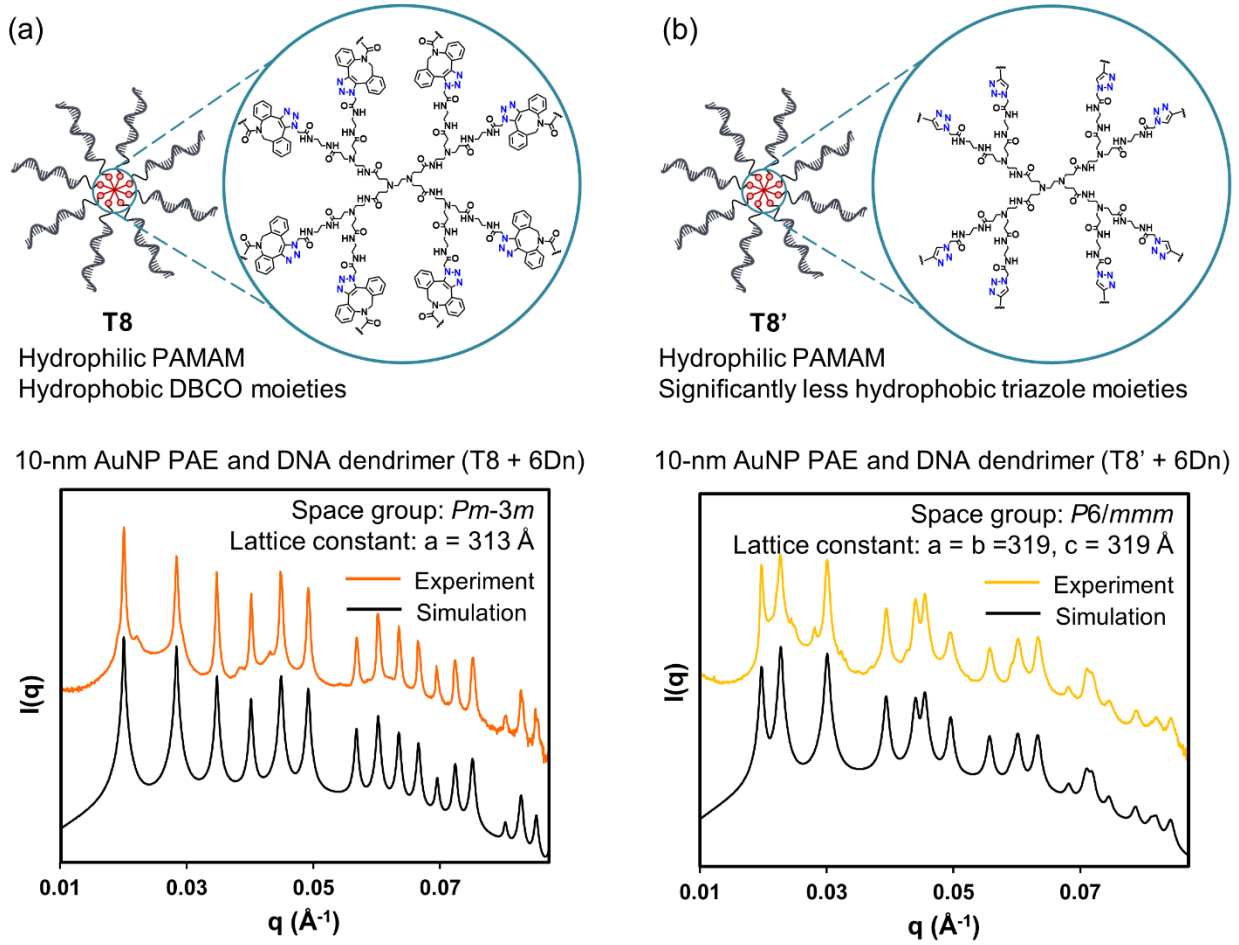

Figure S7. The influence of hydrophobic moieties on dendrimer-dendrimer association and ultimately the superlattice crystal structure. Above: the molecular core and conjugation moieties of (a) T8 (DBCO moieties) and (b) T8' (hexynyl moieties) are highlighted. Below: experimental (colored) and simulated (black) SAXS spectra of nanoparticle superlattices synthesized using (a) T8-templated dendrimer (DBCO moieties) and (b) T8'-templated dendrimer (hexynyl moieties). Both assemblies are prepared with 0.5 M NaCl, 10 mM phosphate, 0.015% SDS, pH 7.4 buffer.

3D Models of DNA Dendrimers and Micelle-Dendrimers

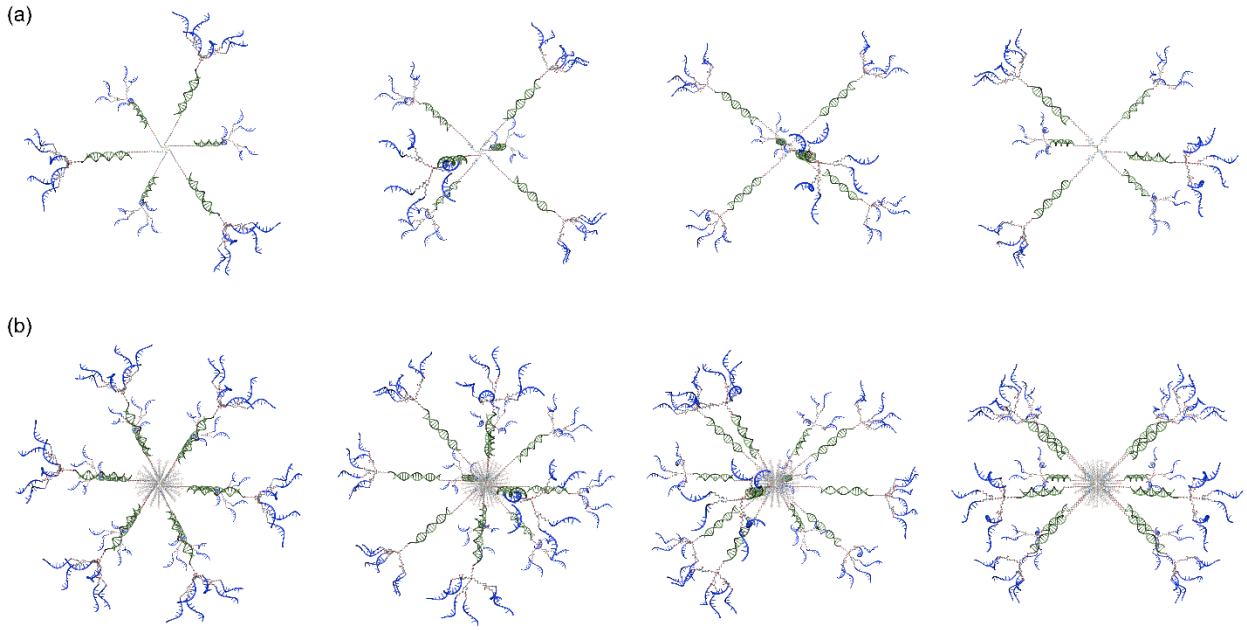

Figure S8. (a) 3D models of a DNA dendrimer (a six-arm templated combined with six copies of six-branch dendrons), rotated by a 30° interval from left to right. (b) 3D models of a DNA micelle-dendrimer made up of two DNA dendrimers and a SDS micelle, rotated by a 30° interval from left to right. The SDS micelles and the DNA dendrimers were drawn to scale. Models were created using Cinema 4D™.

Additional SAXS Data Showing the Effect of SDS Concentration

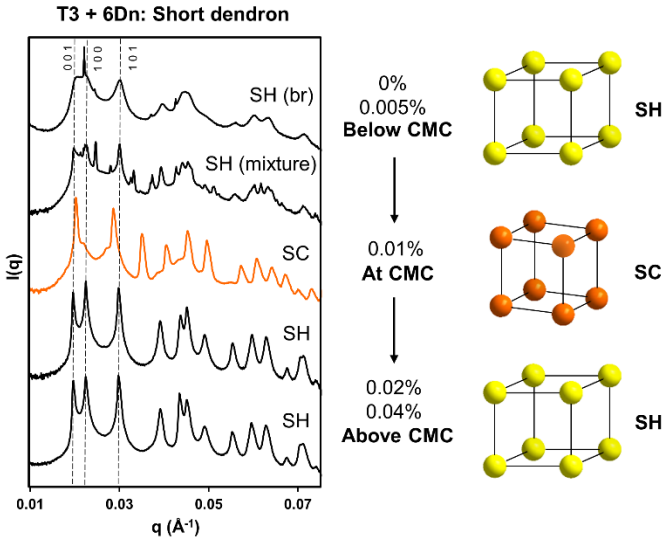

Figure S9. 10-nm AuNP PAEs were combined with DNA dendrimers made up of T3 and 6Dn (short stem). 0.2 µM of T3 and 0.6 µM of 6Dn were used, identical to the conditions in Figure 3b. From top to bottom: SAXS traces collected at 0, 0.005, 0.01, 0.02, and 0.04% SDS. The short dendron stem limits the degree of

dendrimer-dendrimer association, and thus the SC phase was formed instead of the Ti_5Ga_4-type phase, at 0.01% SDS, as in the case of colloidal crystals prepared using DNA dendrimers made up of T3 and 6Dn-L2.

The Effect of Dendron Stem Length on Dendrimer Association

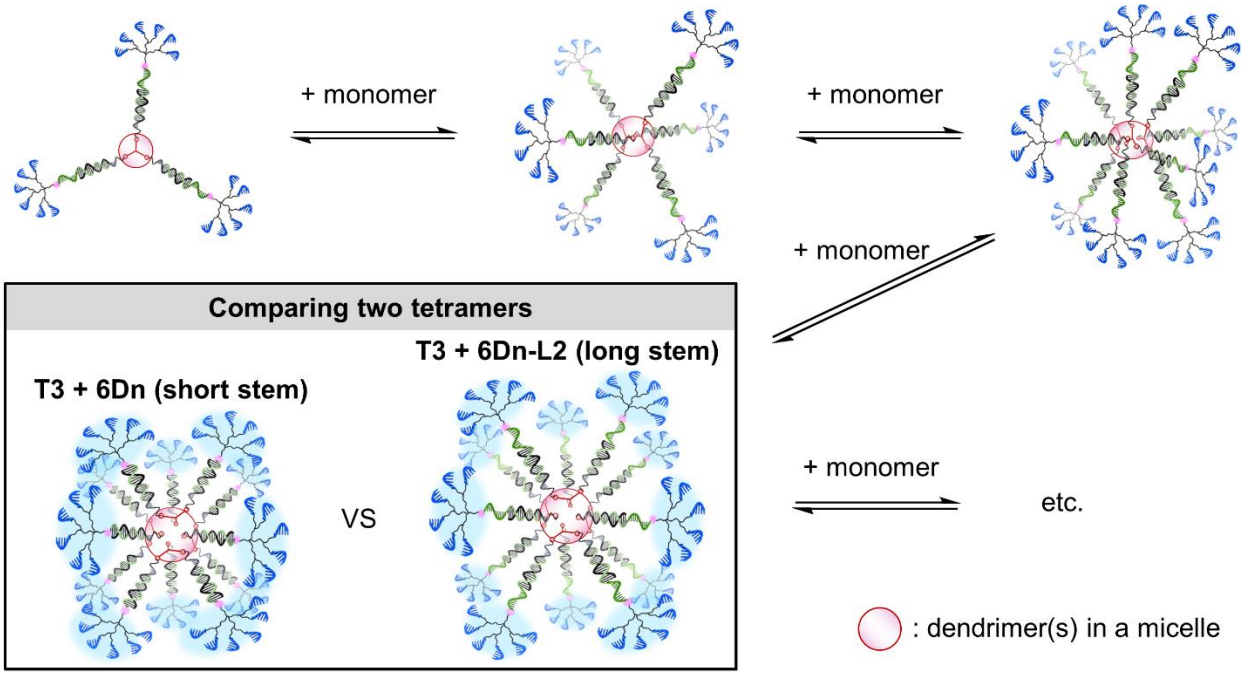

Figure S10. A 2D model depicting the impact of dendron stem length on the degree of dendrimer-dendrimer association in the presence of SDS micelles. A longer stem relieves steric hindrance between dendron branches in a multi-mer. Thus, a longer dendron stem would enable a higher degree of dendrimer-dendrimer association and affect the resulting colloidal crystal structures.

Analysis of Coordination Distances and Packing Densities

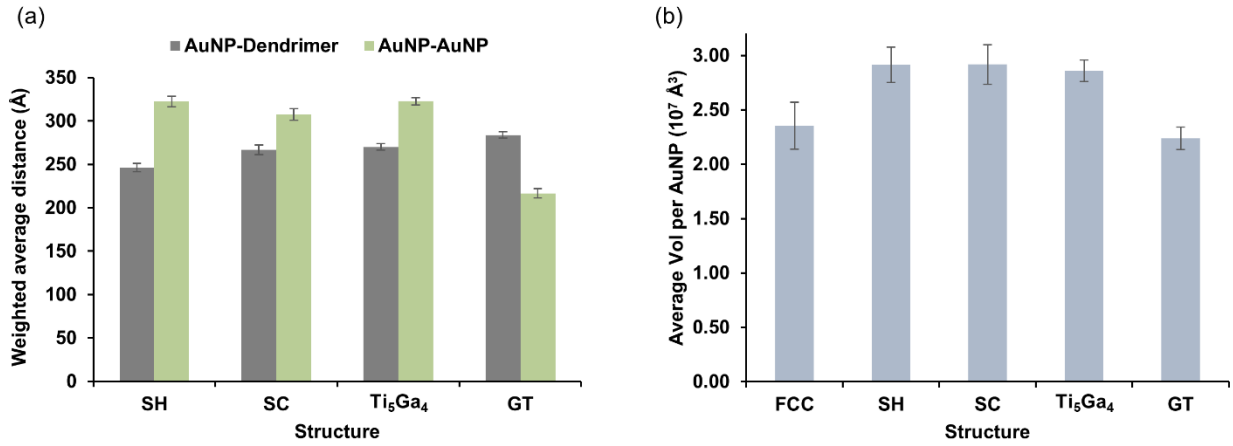

Figure S11. (a) Weighted average distances, in the first coordination sphere, between DNA micelle-dendrimers and AuNPs (first, grey), and between AuNPs and AuNPs (second, green). n is the number of independently characterized structures. An increase in the average first-coordination distance between complementary particles (dark grey) indicates an increase in the average size of the DNA micelle-dendrimers that template that structure. SH: 246 ± 4.6 Å, 322 ± 6.2 Å, n = 10. SC: 267 ± 5.6 Å, 308 ± 6.6 Å, n = 12. Ti_5Ga_4: 270 ± 3.6 Å, 323 ± 4.3 Å, n = 10. GT: 284 ± 3.6 Å, 217 ± 5.2 Å, n = 7. (b) The average volume of a superlattice structure per AuNP. The low average volume per AuNP (thus a high packing density of AuNPs) in the FCC phase is due to the absence of DNA templates and the structure's metallic bonding character. The high density of AuNPs in the GT phase is due to its A_2B stoichiometry (i.e., for every DNA micelle-dendrimer there are two AuNPs).

Voronoi Polyhedra Analysis

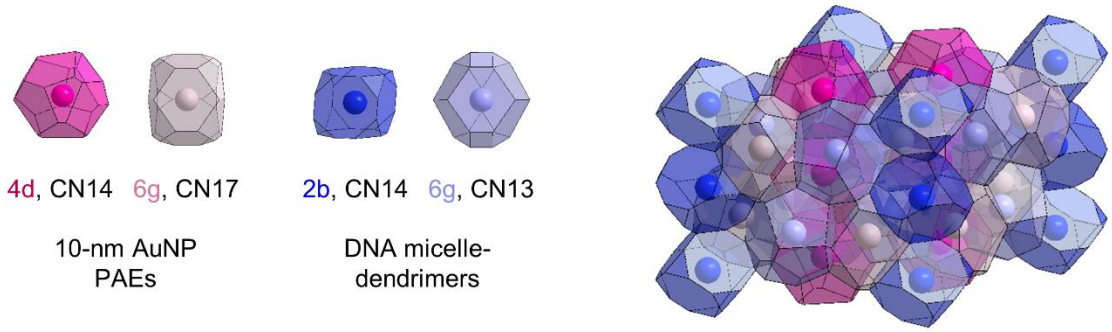

Figure S12. The symmetry-breaking induced by discrete DNA micelle-dendrimers can also be highlighted by constructing a new set of Voronoi polyhedra around both the AuNPs and DNA micelle-dendrimers. Two of these Voronoi polyhedra are Frank-Kasper (FK)-type, with a coordination number (CN) of 14, while the other two are pseudo-FK polyhedra with CNs of 13 and 17, respectively.

Toehold-Mediated Strand Displacement Reactions

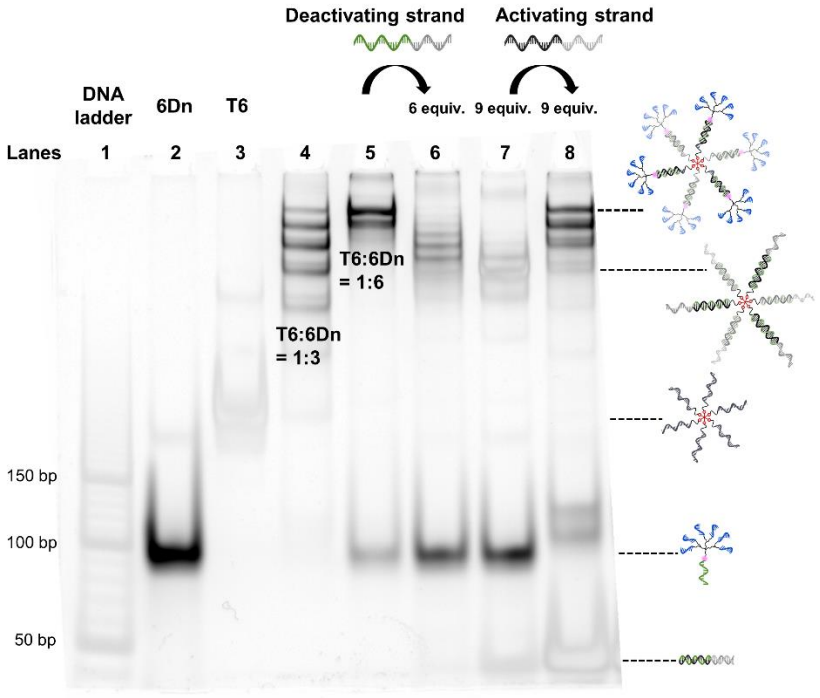

Figure S13. Dendrons and templates are designed to enable toehold-mediated strand displacement reactions. A hybridization-enabled DNA dendrimer PAE can be reconfigured into individual dendron electron equivalents (EEs) using simple DNA strands (deactivating and activating strands) as stimuli. A 4.5% native PAGE showing the effect of adding deactivating strand and activating strand on the size of the resulting constructs. The gel is stained using GelRed and imaged on the Cy3-channel. As a result, the darker bands show the presence of Cy3 label (i.e., dendrons are part of the constructs). Lane 1: O'RangeRuler 10 bp DNA Ladder (ThermoFisher); lane 2: 6Dn; lane 3: T6; lane 4: one equiv. of T6 and three equiv. of 6Dn; lane 5: one equiv. of T6 and six equiv. of 6Dn; lane 6: one equiv. of T6, six equiv. of 6Dn, and six equiv. of

deactivating strand; lane 7: one equiv. of T6, six equiv. of 6Dn, and nine equiv. of deactivating strand; lane 8: one equiv. of T6, six equiv. of 6Dn, nine equiv. of deactivating strand, and nine equiv. of activating strand.

Additional Crystal Structure Reconfiguration

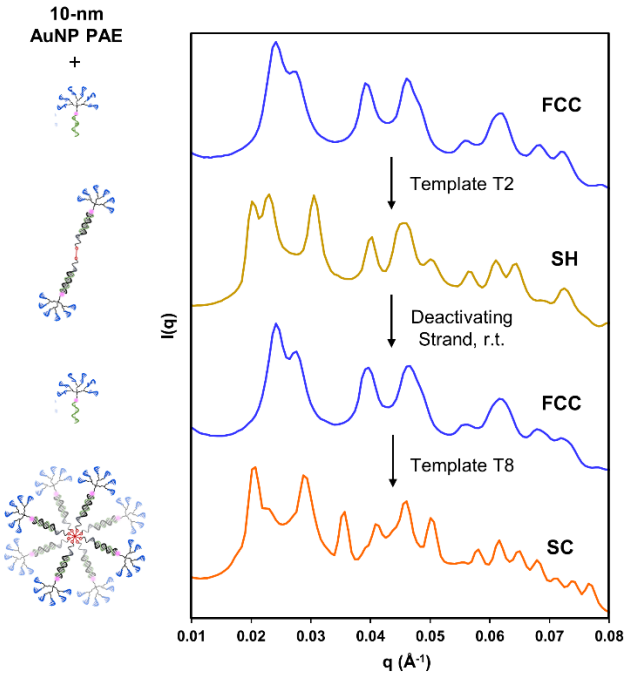

Figure S14. Switching a sample between three crystal structures in one pot. Consecutive additions of the template T2 and the deactivating strand reconfigured the colloidal crystal structures from FCC (blue trace), to SH (yellow trace), and then back to FCC (blue trace). After each of the above additions, the samples were mixed gently *via* pipetting, and they were left at room temperature for 24 h. After the original template (T2) was inactivated by the addition of the deactivating strand, a new template (T8) was added to reconfigure the sample into SC (orange trace) phase, after heating to 60 °C and slow-cooling to 22 °C.

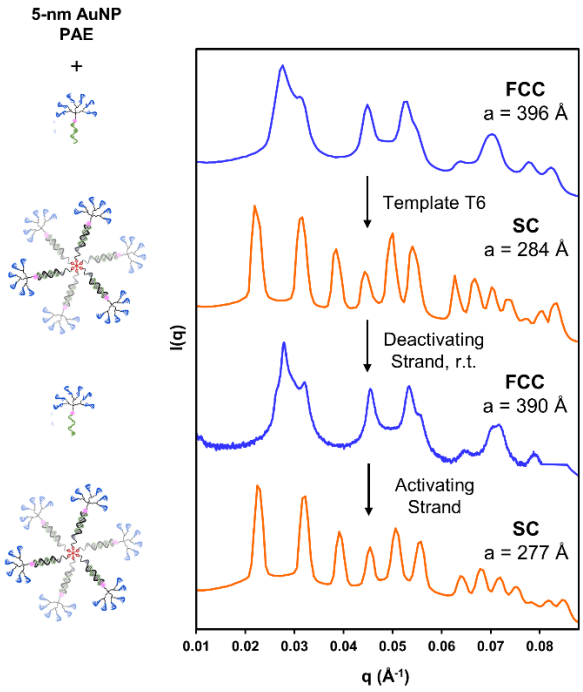

Figure S15. Dendrimer-templated nanoparticle superlattices and structure reconfiguration is also applicable to 5-nm AuNPs. Here, consecutive addition of the template T6, the deactivating strand, and the activating strand allow one to reconfigure the colloidal crystal structures between FCC (blue traces) and SC (orange traces) over two full cycles in one pot. The samples were mixed gently after each addition. The sample is heated to 60 °C and slow-cooled to 22 °C at 0.1°C per min after the addition of the template and the activating strand.

Additional Gel Images

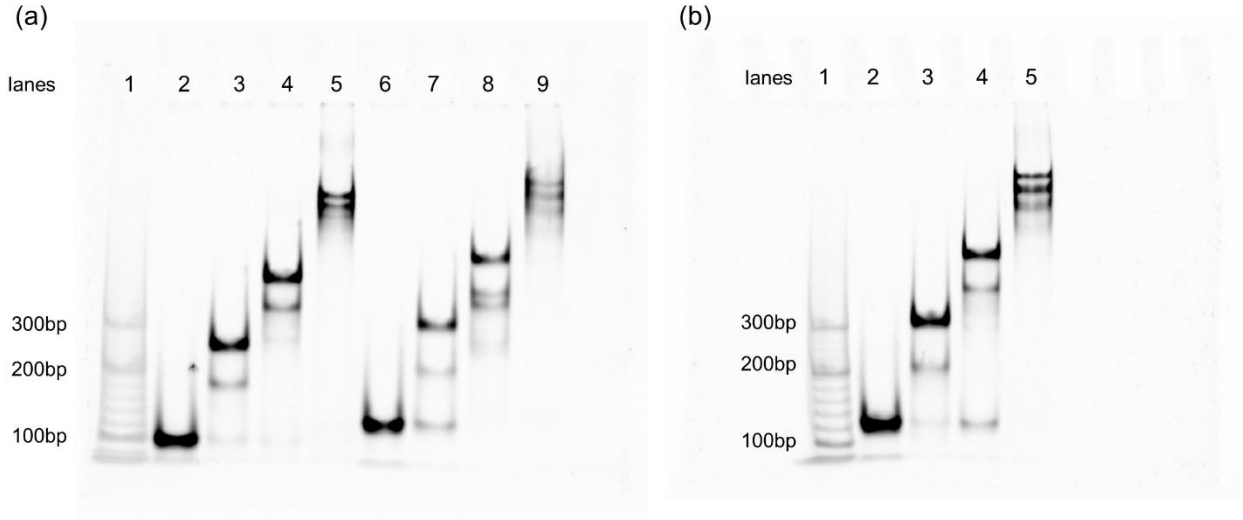

Figure S16. Assembly of DNA dendrons (a) 4Dn and (b) 6Dn with templates (T2, T3, and T6) in 0.5 M NaCl, characterized *via* 5% native polyacrylamide gel electrophoresis (PAGE). The gel is stained using GelRed and imaged on the Cy3 channel. (a) and (b) show the gels in their entirety and correspond to the

left and right gels in Figure 1d, respectively. For (a), lane 1: O'RangeRuler 20 bp DNA Ladder (ThermoFisher); lane 2: 4Dn, lane 3: one equiv. of T2 and two equiv. of 4Dn, lane 4: one equiv. of T3 and three equiv. of 4Dn, lane 5: one equiv. of T6 and six equiv. of 4Dn, lane 6: 6Dn, lane 7: one equiv. of T2 and two equiv. of 6Dn, lane 8: one equiv. of T3 and three equiv. of 6Dn, lane 9: one equiv. of T6 and six equiv. of 6Dn. Lanes 7 to 9 of (a) was slightly underloaded in 6Dn. For (b), lane 1: O'RangeRuler 20 bp DNA Ladder (ThermoFisher); lane 2: 6Dn, lane 3: one equiv. of T2 and two equiv. of 6Dn, lane 4: one equiv. of T3 and three equiv. of 6Dn, lane 5: one equiv. of T6 and six equiv. of 6Dn. Lane 5 of (b) was underloaded in 6Dn.

Small-Angle X-Ray Scattering (SAXS) Indexing and Simulations

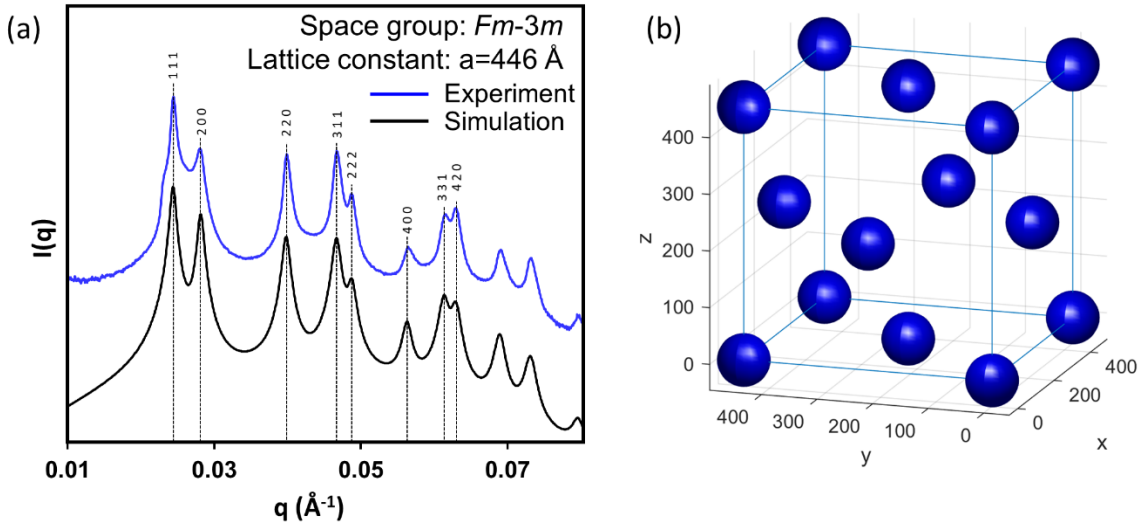

Figure S17. (a) Azimuthally averaged 1D SAXS spectra of a representative FCC phase (blue: experiment, black: simulation). These are identical to the spectra shown in Figure 2b. The first eight scattering peaks and their corresponding Miller indices (*hkl*) are labeled (black dashed lines). (b) Structural model of AuNP sublattice in FCC phase symmetry used to generate the simulated spectrum.

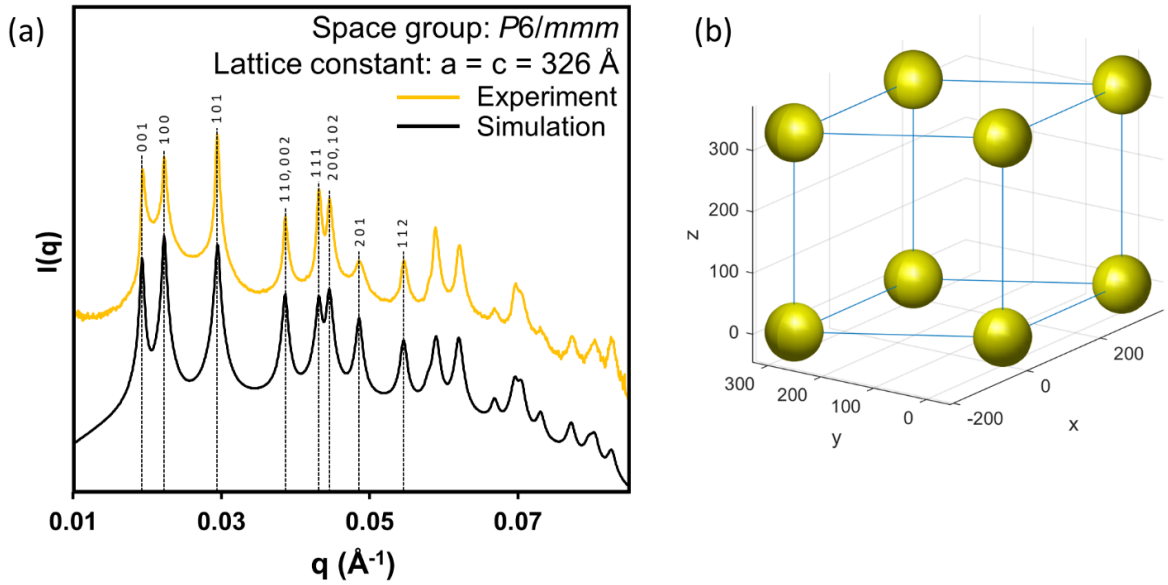

Figure S18. (a) Azimuthally averaged 1D SAXS spectra of a representative SH phase (yellow: experiment, black: simulation). These are identical to the spectra shown in Figure 2c. The first eight scattering peaks and their corresponding Miller indices (*hkl*) are labeled (black dashed lines). (b) The structural model of the AuNP sublattice in SH phase symmetry used to generate the simulated spectrum.

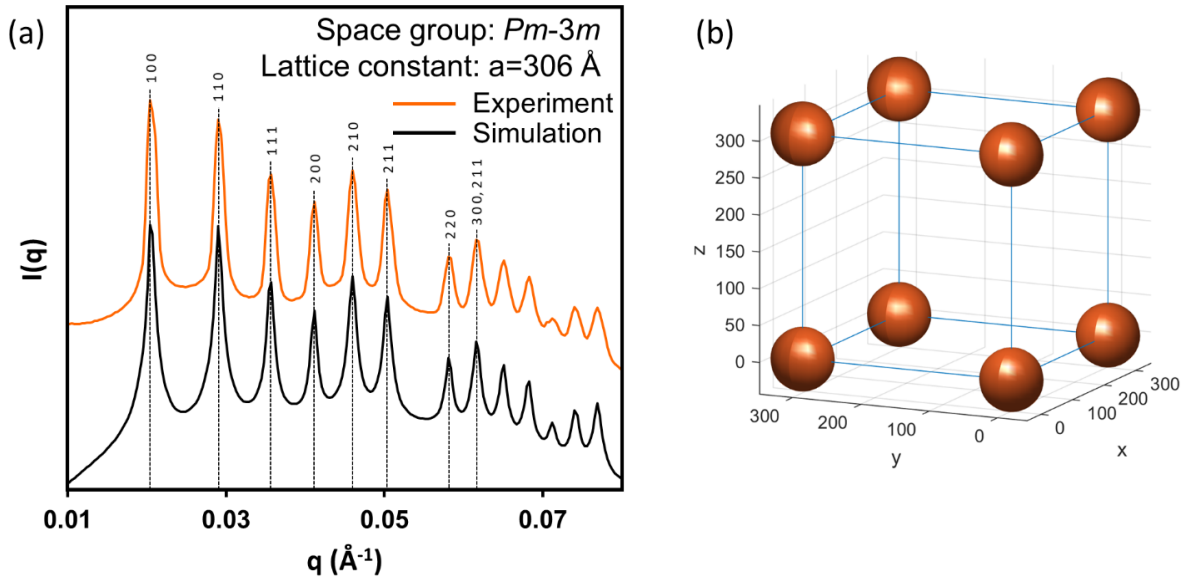

Figure S19. (a) Azimuthally averaged 1D SAXS spectra of a representative SC phase (orange: experiment, black: simulation). These are identical to the spectra shown in Figure 2d. The first eight scattering peaks and their corresponding Miller indices (*hkl*) are labeled (black dashed lines). (b) The structural model of the AuNP sublattice in SC phase symmetry used to generate the simulated spectrum.

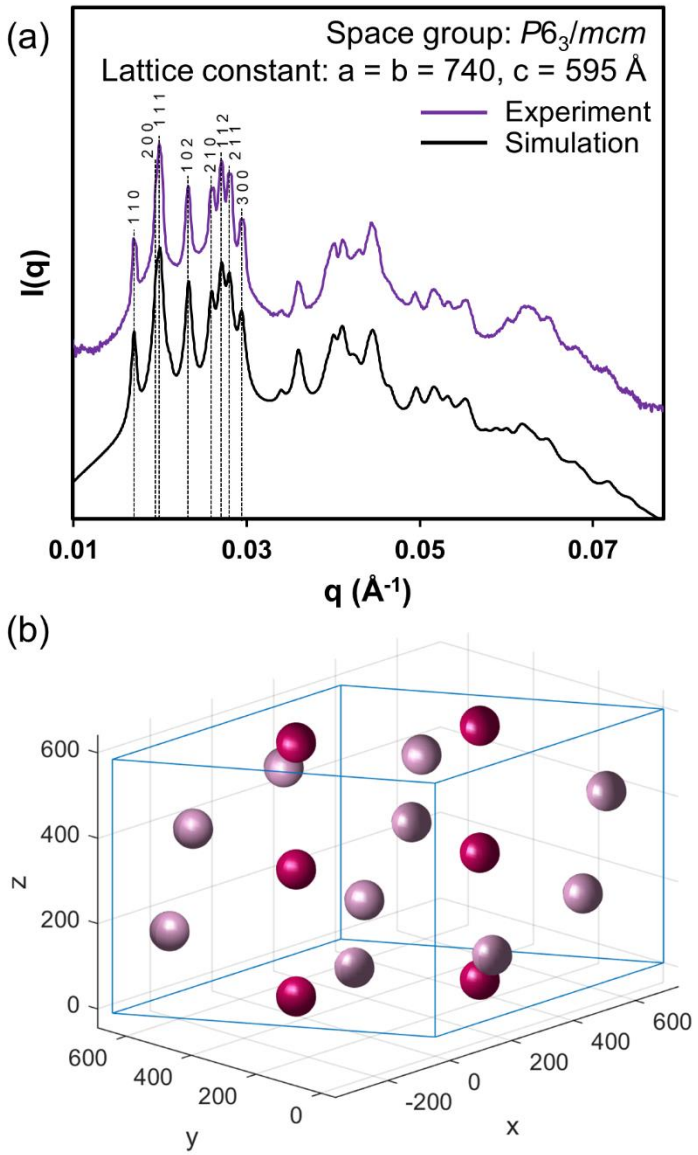

Figure S20. (a) Azimuthally averaged 1D SAXS spectra of a representative Ti_5Ga_4-type phase (purple: experiment, black: simulation). These are identical to the spectra shown in Figure 2e. The first eight scattering peaks and their corresponding Miller indices (*hkl*) are labeled (black dashed lines). (b) The structural model of the AuNP sublattice in Ti_5Ga_4-type phase symmetry used to generate the simulated spectrum.

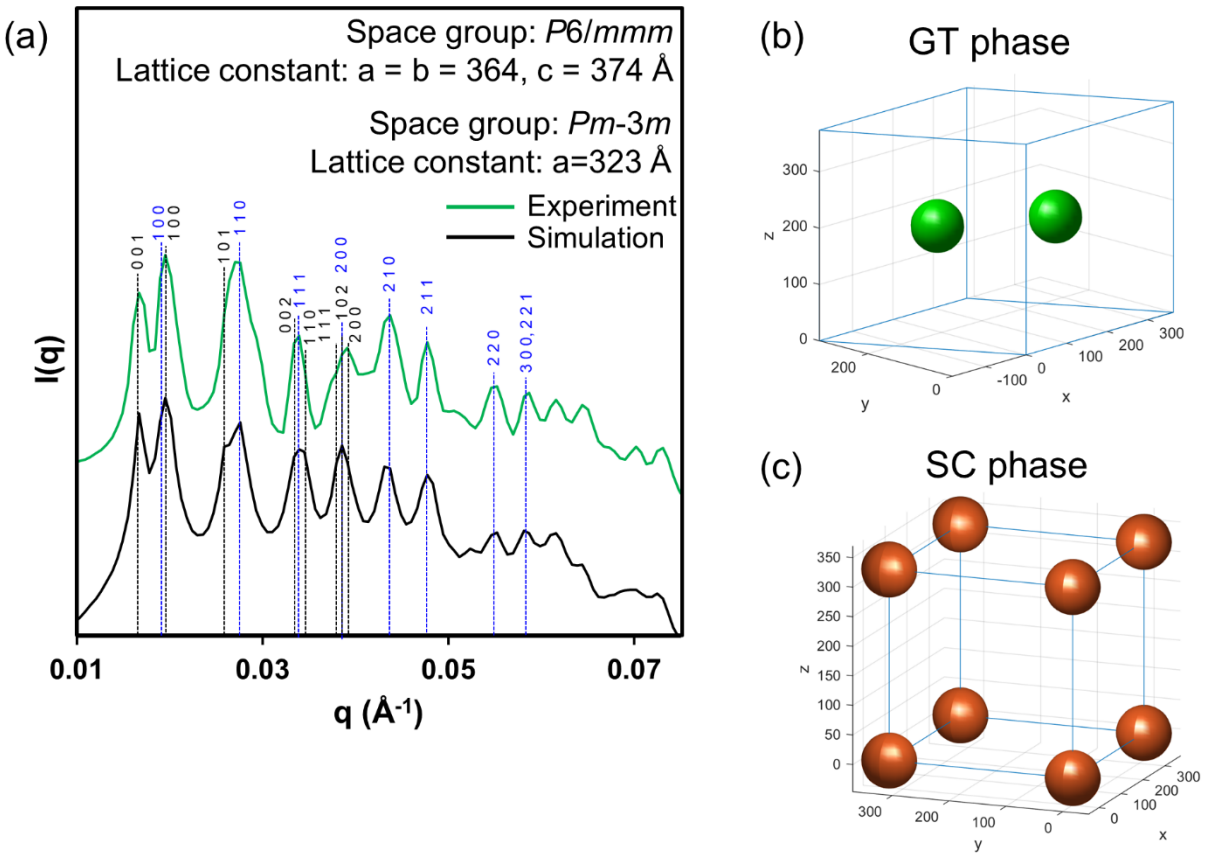

Figure S21. (a) Azimuthally averaged 1D SAXS spectra of a representative mixture of GT and SC phases (green: experiment, black: simulation of GT phase). These are identical to the spectra shown in Figure 2f. For each phase, the first eight scattering peaks and their corresponding Miller indices (*hkl*) are labeled (black dashed lines for GT phase and blue dashed lines for SC phase). The structural models of the AuNP sublattice in (b) GT and (c) SC phase symmetries used to generate the simulated spectrum.

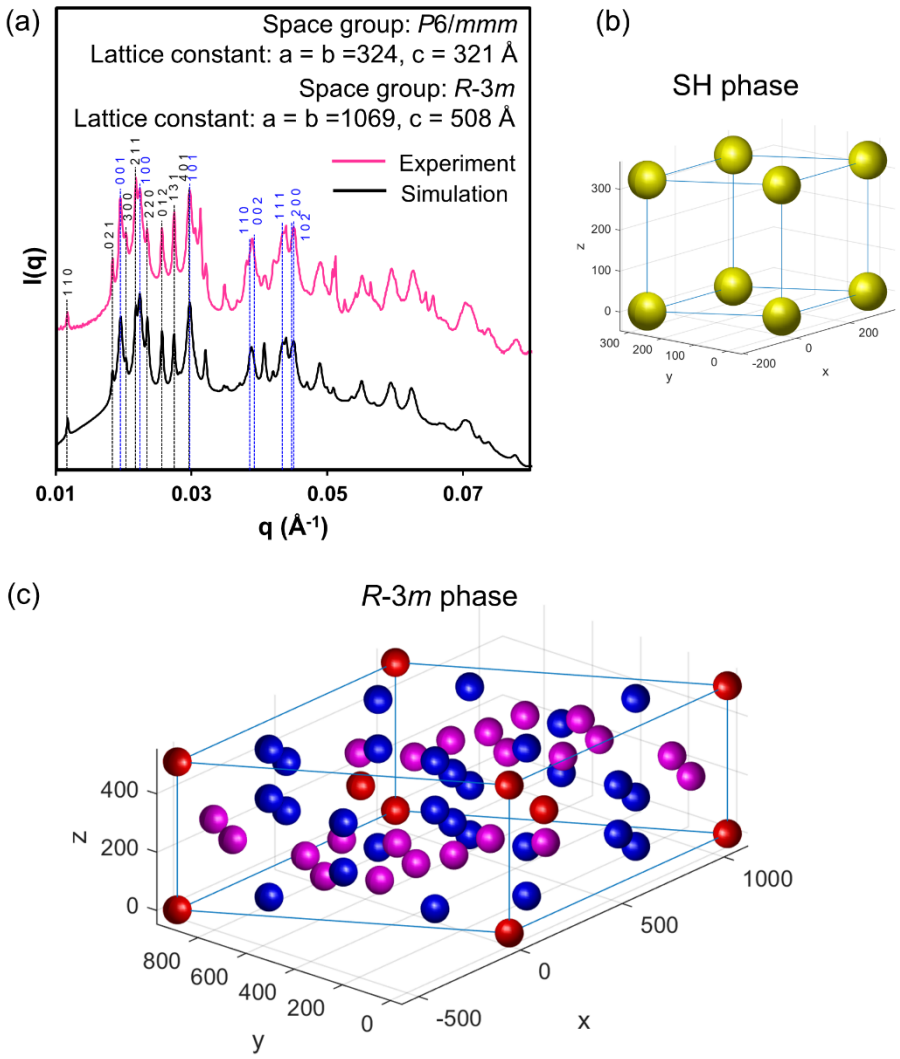

Figure S22. (a) Azimuthally averaged 1D SAXS spectra of a representative mixture of a SH phase and a partially disordered *R*-3*m* phase (pink: experiment, black: simulation). These are identical to the spectra shown in Figure S3. The first eight scattering peaks and their corresponding Miller indices (*hkl*) are labeled (black dashed lines for SH phase and blue dashed lines for partially disordered *R*-3*m* phase). The structural models of the AuNP sublattice in (b) SH and (c) partially disordered *R*-3*m* phase symmetries used to generate the simulated spectrum. All AuNP positions (including partially occupied ones) are depicted in the latter image.

Additional Electron Micrographs

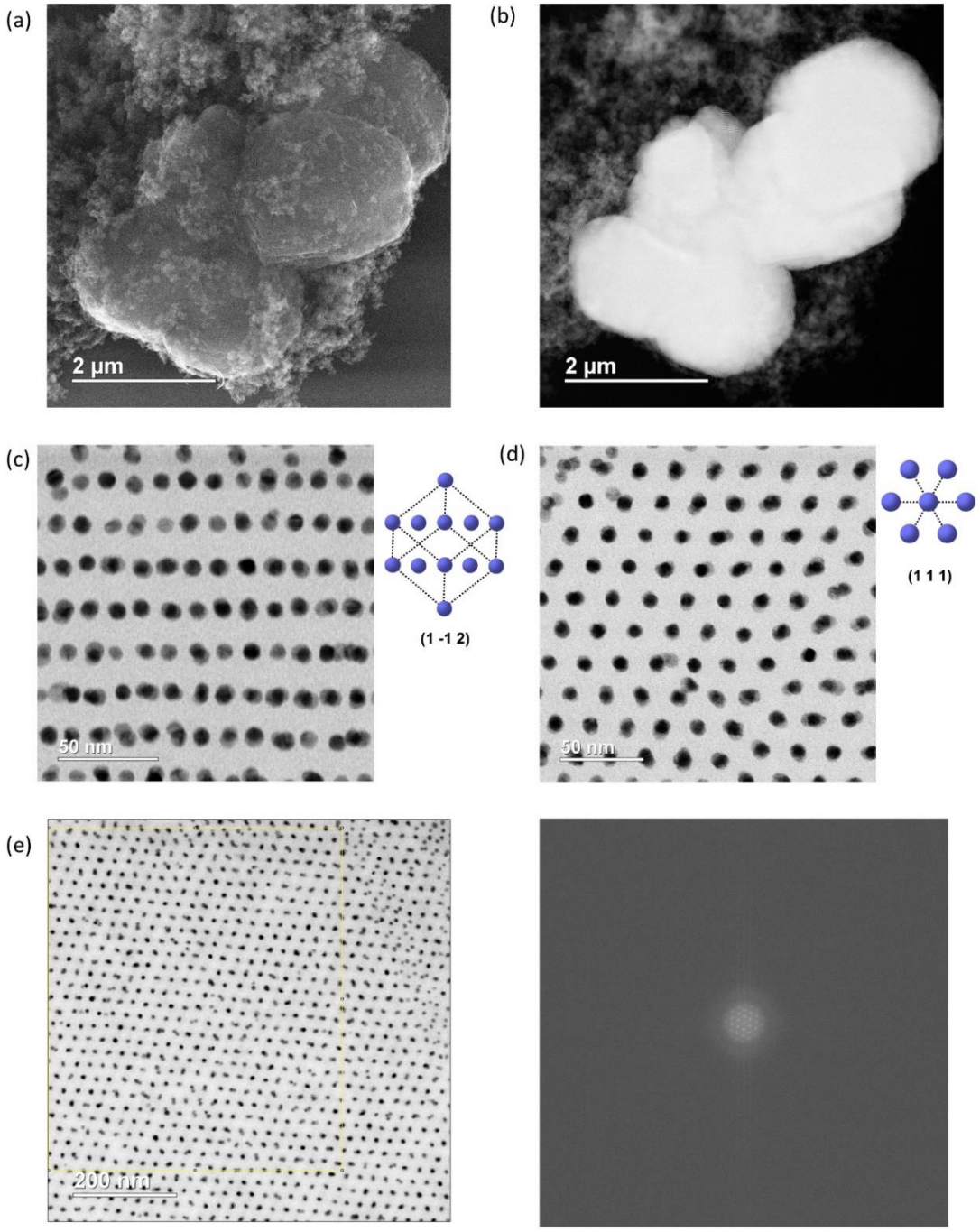

Figure S23. (a) Representative SE-STEM and (b) ADF-STEM images of FCC phase crystals after silica encapsulation. Cross-sectional ABF-STEM image and 2D projection of the structural model (dotted black line represents unit cell edges) along the (c) [1 -1 2] and (d) [1 1 1] zone axes of a ultramicrotomed FCC phase superlattice. The latter is the uncropped version of the electron micrograph shown in Figure 2b. (e) The boxed region of a low-magnification ABF-STEM image (left) was Fourier-transformed to yield a diffractogram (right).

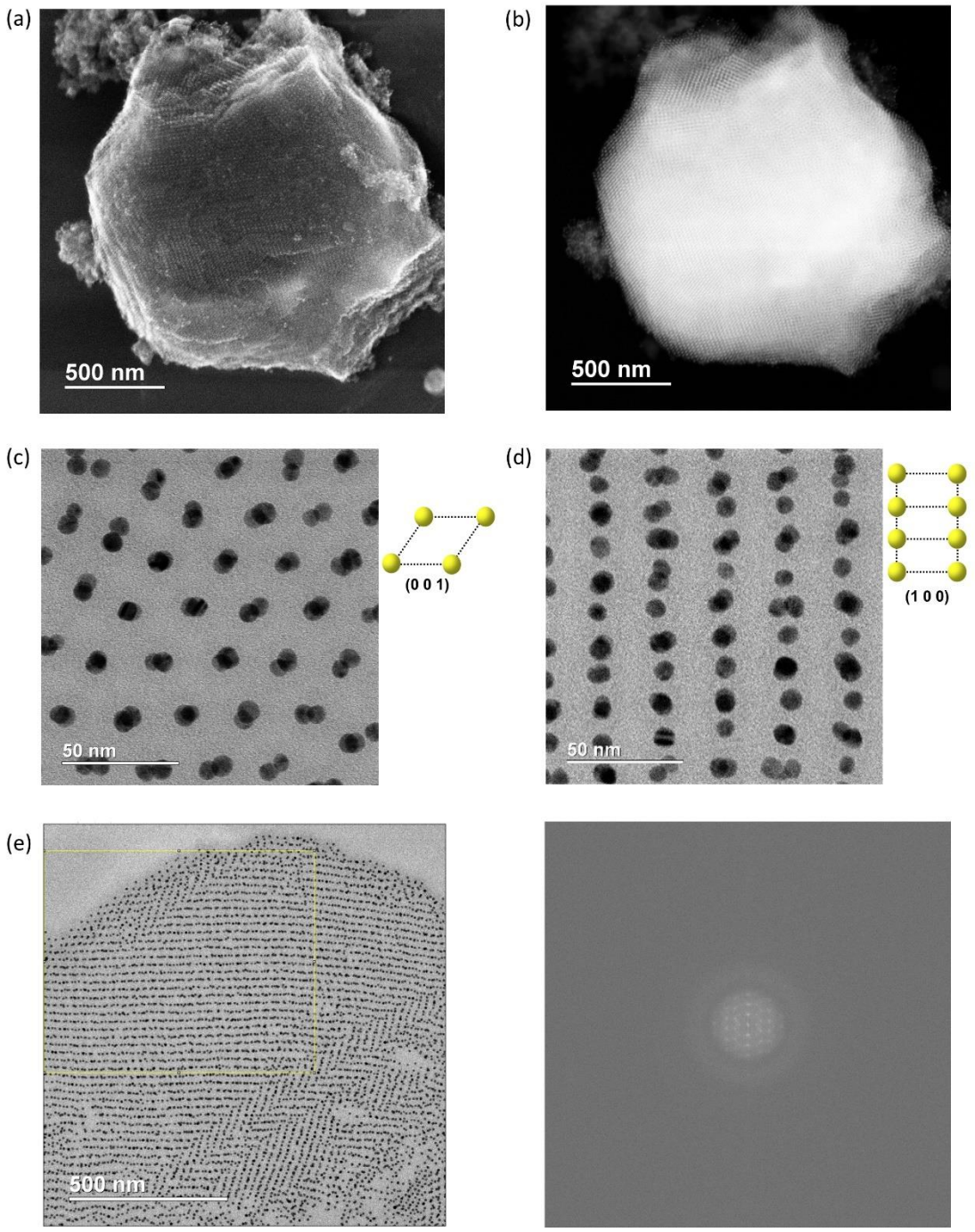

Figure S24. (a) Representative SE-STEM and (b) ADF-STEM images of an SH phase crystal after silica encapsulation. The shape of the crystal is roughly hexagonal as the SH phase has multiple lattice planes with hexagonal patterns. Cross-sectional ABF-STEM image and 2D projection of the structural model (dotted black line represents unit cell edges) along the (c) [0 0 1] and (d) [1 0 0] zone axes of a ultramicrotomed SH phase superlattice. The latter is the uncropped version of the electron micrograph shown in Figure 2c. (e) The boxed region of a low-magnification ABF-STEM image (left) was Fourier-transformed to yield a diffractogram (right).

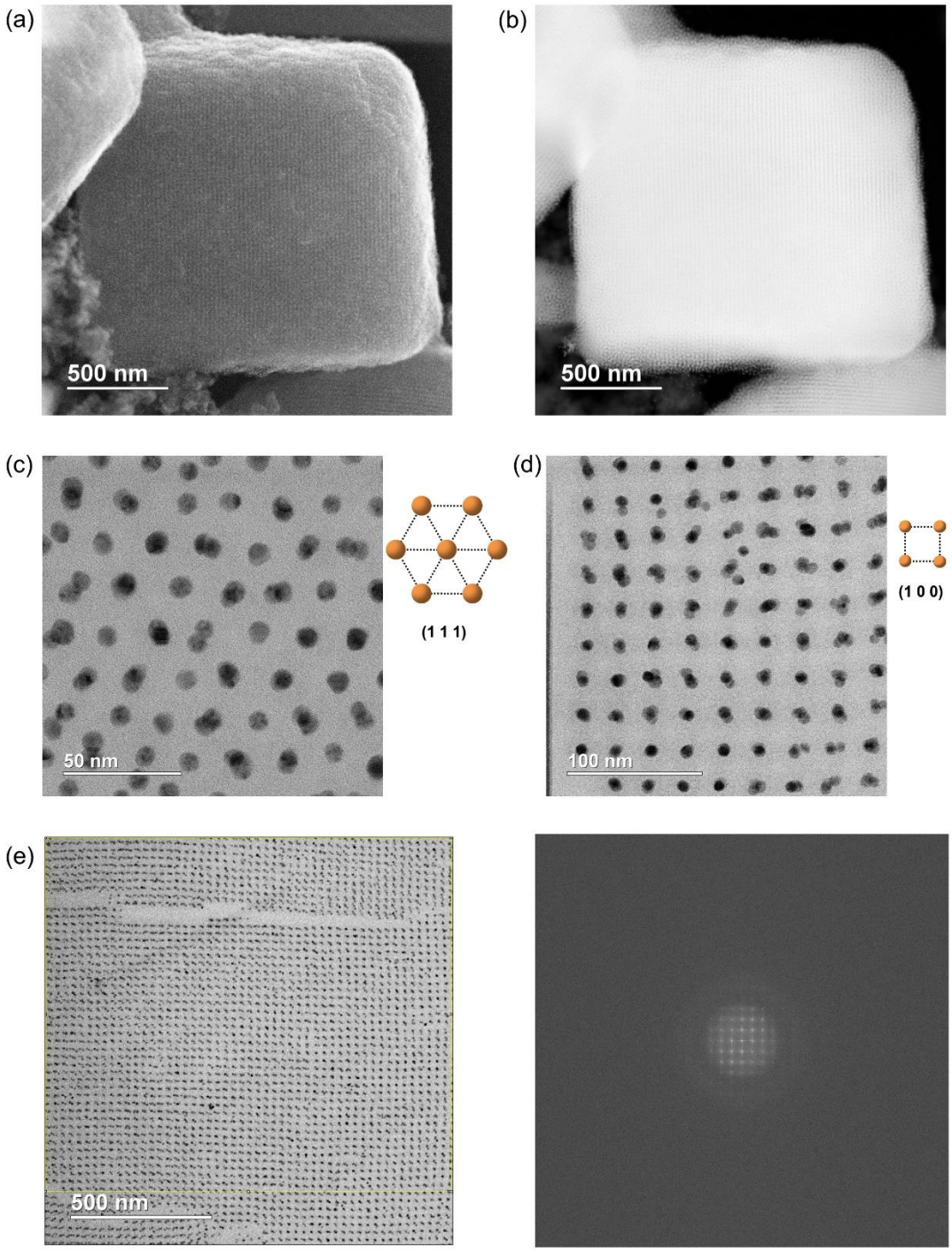

Figure S25. (a) Representative SE-STEM and (b) ADF-STEM images of a SC phase crystal after silica encapsulation. The cubic shape of the crystal reflects its simple cubic symmetry. Cross-sectional ABF-STEM image and 2D projection of the structural model (dotted black line represents unit cell edges) along the (c) [1 1 1] and (d) [1 0 0] zone axes of a ultramicrotomed SC phase superlattice. The latter is the uncropped version of the electron micrograph shown in Figure 2d. (e) The boxed region of a low-magnification ABF-STEM image (left) was Fourier-transformed to yield a diffractogram (right).

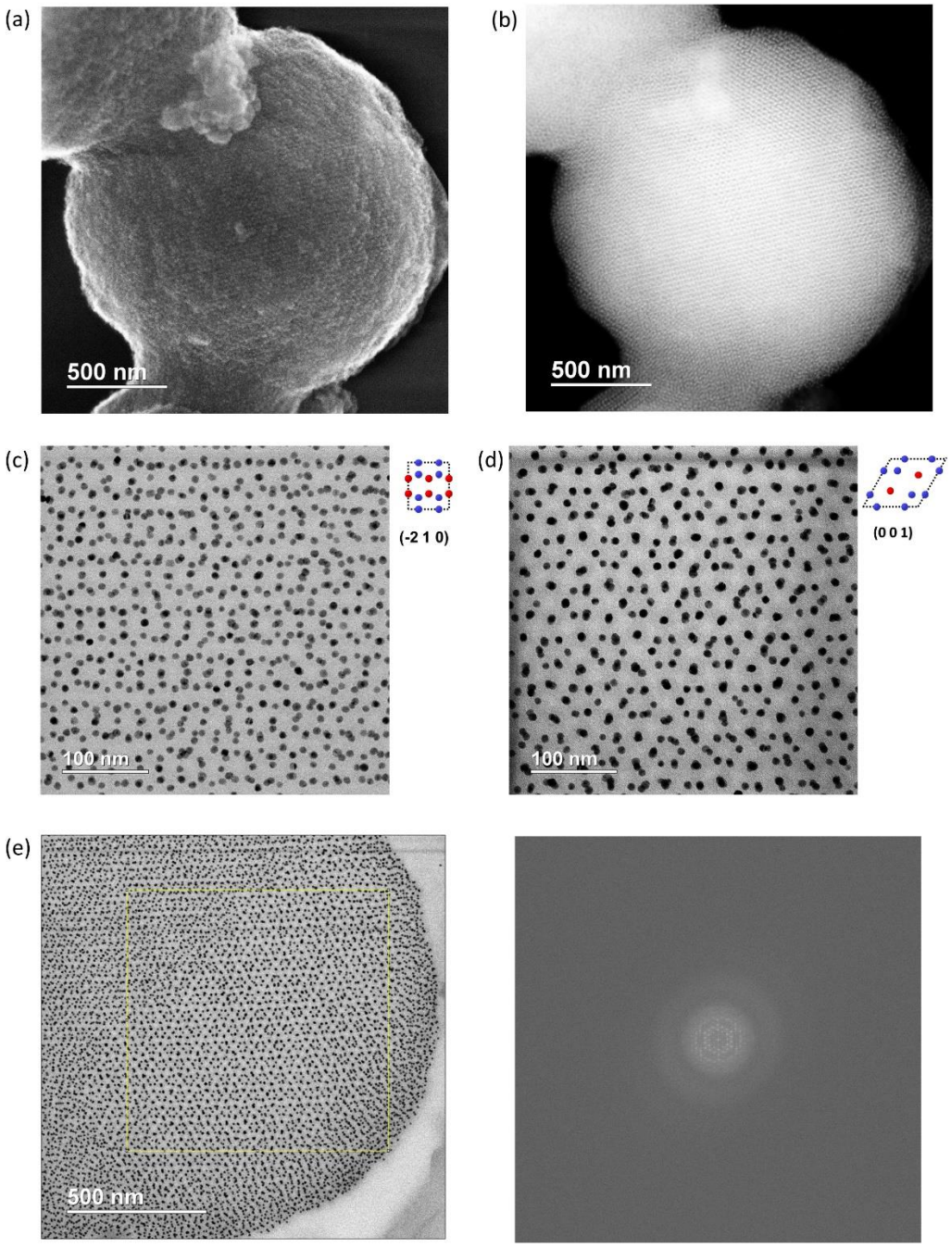

Figure S26. (a) Representative SE-STEM and (b) ADF-STEM images after silica encapsulation of a Ti_5Ga_4-type phase crystal. Due to the Ti_5Ga_4-type phase's low symmetry, the crystals do not present any particular low-energy facets and thus grow to form non-faceted, spherical micro-crystallites. Cross-sectional ABF-STEM image and 2D projection of the structural model (red: 4d, blue: 6g, dotted black line represents unit cell edges) along the (c) [-2 1 0] and (d) [0 0 1] zone axes of a ultramicrotomed Ti_5Ga_4-type phase superlattice. The latter is the uncropped version of the electron micrograph shown in Figure 2e. (e) The boxed region of a low-magnification ABF-STEM image (left) was Fourier-transformed to yield a diffractogram (right).

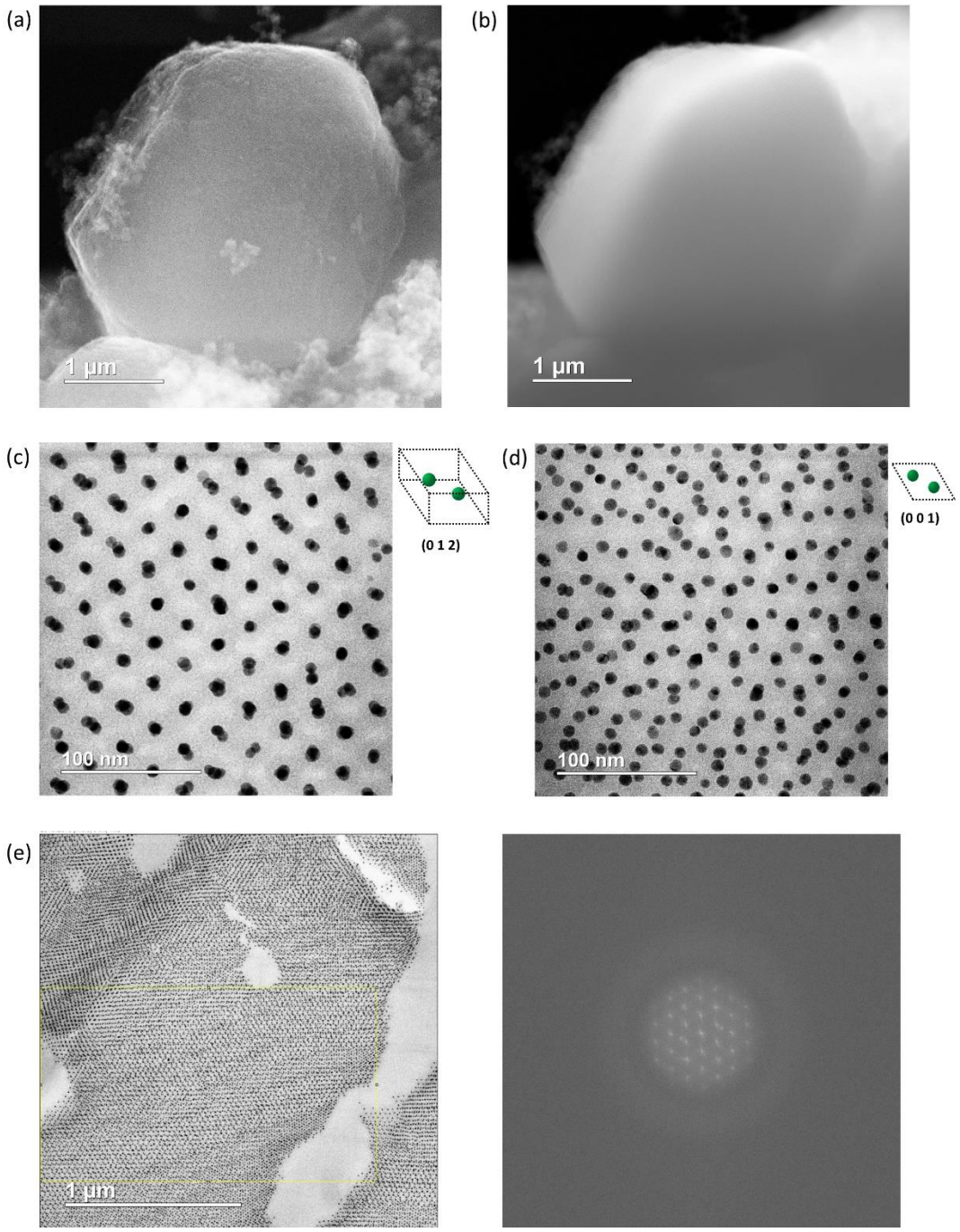

Figure S27. (a) Representative SE-STEM and (b) ADF-STEM images of a GT phase crystal after silica encapsulation. The shape of the crystal is roughly hexagonal as the GT phase has multiple lattice planes with hexagonal patterns. Cross-sectional ABF-STEM image and 2D projection of the structural model (dotted black line represents unit cell edges) along the (c) [0 1 2] and (d) [0 0 1] zone axes of a ultramicrotomed GT phase superlattice. The latter is the uncropped version of the electron micrograph shown in Figure 2f. (e) The boxed region of a low-magnification ABF-STEM image (left) was Fourier-transformed to yield a diffractogram (right).

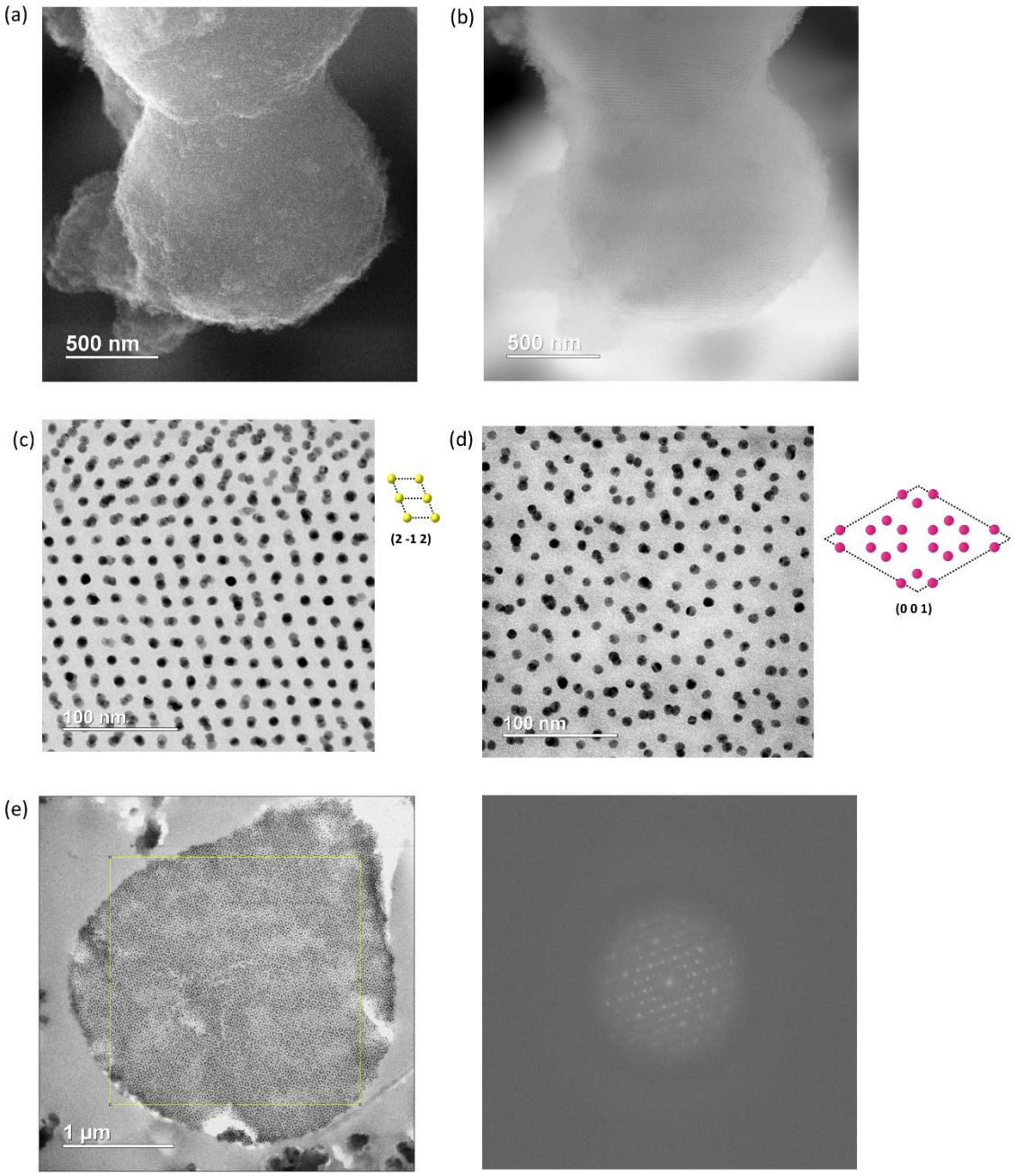

Figure S28. (a) Representative SE-STEM and (b) ADF-STEM images of the partially disordered *R*-3*m* phase crystals after silica encapsulation. Due to *R*-3*m*'s low symmetry, the crystals do not present any particular low-energy facets and thus grow to form non-faceted, spherical micro-crystallites. The colloidal crystal sample is comprised of nanoparticle superlattices in SH and partially disordered *R*-3*m* phases. Cross-sectional ABF-STEM image and 2D projection of the structural model (dotted black line represents unit cell edges) along the (c) [2 -1 2] zone axis of a ultramicrotomed SH phase superlattice and (d) along the [0 0 1] zone axis of a ultramicrotomed *R*-3*m*phase superlattice. The latter is the uncropped version of the electron micrograph shown in Figure S3. (e) The boxed region of a low-magnification ABF-STEM image (left) was Fourier-transformed to yield a diffractogram (right).

Supplementary References

1. Distler, M. E.; Teplensky, M. H.; Bujold, K. E.; Kusmierz, C. D.; Evangelopoulos, M.; Mirkin, C. A. DNA Dendrons as Agents for Intracellular Delivery. *J. Am. Chem. Soc.* **2021**, *143*, 13513−13518.
2. Thaner, R. V.; Eryazici, I.; Farha, O. K.; Mirkin, C. A.; Nguyen, S. B. T. Facile one-step solid-phase synthesis of multi-topic organic-DNA hybrids via "click" chemistry. *Chem. Sci.* **2014**, *5*, 1091−1096.
3. Cheng, H. F.; Wang, S.; Mirkin, C. A. Electron-Equivalent Valency through Molecularly Well-Defined Multivalent DNA. *J. Am. Chem. Soc.* **2021**, *143*, 1752−1757.
4. Li, T.; Senesi, A. J.; Lee, B. Small Angle X-ray Scattering for Nanoparticle Research. *Chem. Rev.* **2016**, *116*, 11128−11180.
5. Auyeung, E.; Macfarlane, R. J.; Choi, C. H. J.; Cutler, J. I.; Mirkin, C. A. Transitioning DNA-Engineered Nanoparticle Superlattices from Solution to the Solid State. *Adv. Mater.* **2012**, *24*, 5181−5186.
6. Zadeh, J. N.; Steenberg, C. D.; Bois, J. S.; Wolfe, B. R.; Pierce, M. B.; Khan, A. R.; Dirks, R. M.; Pierce, N. A. NUPACK: analysis and design of nucleic acid systems. *J. Comput. Chem.* **2011**, *32*, 170−173.
7. Hayashi, S.; Ikeda, S. Micelle size and shape of sodium dodecyl sulfate in concentrated sodium chloride solutions. *J. Phys. Chem.* **1980**, *84*, 744−751.
8. Schubert, K.; Meissner, H. G.; Poetzschke, M.; Rossteutscher, W.; Stolz, E. Structure data on metallic phases. VII. *Naturwissenschaften* **1962**, *49*, 57.
9. Rieger, W.; Nowotny, H.; Benesovsky, F. Phases with octahedral units of transition metals. *Monatsh. Chem.* **1965**, *96*, 232−241.
10. Girard, M.; Wang, S.; Du, J. S.; Das, A.; Huang, Z.; Dravid, V. P.; Mirkin, C. A.; Olvera de la Cruz, M. Particle analogs of electrons in colloidal crystals. *Science* **2019**, *364*, 1174−1178.
11. Jin, R.; Wu, G.; Li, Z.; Mirkin, C. A.; Schatz, G. C. What controls the melting properties of DNA-linked gold nanoparticle assemblies? *J. Am. Chem. Soc.* **2003**, *125*, 1643−1654.